Dephosphorylation of 4EBP1/2 Induces Prenatal Neural Stem Cell Quiescence

Laura C. Geben[1,2], Asa A. Brockman[2], Mary Bronwen L. Chalkley[2], Serena R. Sweet[3], Julia E. Gallagher[2], Alexandra L. Scheuing[2], Richard B. Simerly[3,8], Kevin C. Ess[2,4,8], Jonathan M. Irish[2,5,7], & Rebecca A. Ihrie[2,6,7,8]*

*Correspondence: rebecca.ihrie@vanderbilt.edu

AFFILIATIONS:

1 Program in Pharmacology, Vanderbilt University, Nashville, TN, 37235, USA

2 Department of Cell and Developmental Biology, Vanderbilt University, Nashville, TN, 37235, USA

3 Department of Molecular Physiology and Biophysics, Vanderbilt University, Nashville, TN 37235, USA

4 Department of Pediatrics, Vanderbilt University Medical Center, Nashville, TN 37235, USA

5 Department of Pathology, Microbiology and Immunology, Vanderbilt University Medical Center, Nashville, TN 37235, USA

6 Department of Neurological Surgery, Vanderbilt University Medical Center, Nashville, TN 37235, USA

7 Vanderbilt-Ingram Cancer Center, Vanderbilt University Medical Center, Nashville, TN 37235, USA

8 Vanderbilt Brain Institute, Vanderbilt University, Nashville TN 37235, USA

Contributions

LCG: conceptualization, data acquisition, funding acquisition, data analysis & interpretation, writing – original drafts & final version

AAB: data analysis

MBLC: data acquisition

SRS: data acquisition, data analysis

JEG: data analysis

ALS: data acquisition

RBS: supervision

KCE: conceptualization, supervision, funding acquisition

JMI: supervision, data analysis

RAI: conceptualization, supervision, funding acquisition, data analysis & interpretation, writing – original drafts & final version

29 All authors: review & approval of manuscript

Acknowledgements

The authors would like to acknowledge the members of the Ihrie and Irish laboratories at Vanderbilt University and the members of the Ess laboratory at Vanderbilt University Medical Center for their helpful feedback on experiments and data interpretation throughout the duration of this project. Additionally, we acknowledge the staff of the Translational Pathology Shared Resource (supported by the NIH P30 CA68485 grant), Cell Imaging Shared Resource (supported by NIH grants CA68485, DK20593, DK58404, DK59637 and EY08126), Flow Cytometry Shared Resource (supported by the NIH P30 CA68485 grant and the Vanderbilt Digestive Disease Research Center grant DK058404), and Jose Maldonado at the Neurovisualization Lab at Vanderbilt University and Vanderbilt University Medical Center for their work and expertise in completing these experiments. We gratefully acknowledge the work of Moesha Parsons in sectioning mouse brains and Michael Martland for his work testing antibodies for use in immunostaining.

Funding Information

This research was supported by the following funding resources: NIH T32 GM07628 (LCG), NIH F31 NS120608 (LCG), NIH T32 HD007502 (MBLC), NIH F31 HD106890 (SRS), NIH R01 DK106476 (RBS), NIH R01 NS118580 (KCE, RAI, MBLC), Ben & Catherine Ivy Foundation (RAI), NIH R01 NS096238 (R.A.I., J.M.I.), NIH R01 CA226833 (J.M.I.), NIH U54 CA217450 (J.M.I.), the Michael David Greene Brain Cancer Fund (R.A.I., J.M.I.), the Southeastern Brain Tumor Foundation (R.A.I., J.M.I.), and the Vanderbilt-Ingram Cancer Center (VICC, P30 CA68485).

Abstract

A limiting factor in the regenerative capacity of the adult brain is the abundance and proliferative ability of neural stem cells (NSCs). Adult NSCs are derived from a subpopulation of embryonic NSCs that temporarily enter quiescence during mid-gestation and remain quiescent until postnatal reactivation. Here we present evidence that the mechanistic/mammalian target of rapamycin (mTOR) pathway regulates quiescence entry in embryonic NSCs of the developing forebrain. Throughout embryogenesis, two downstream effectors of mTOR, p-4EBP1/2 T37/46 and p-S6 S240/244, were mutually exclusive in NSCs, rarely occurring in the same cell. While 4EBP1/2 was phosphorylated in stem cells undergoing mitosis at the ventricular surface, S6 was phosphorylated in more differentiated cells migrating away from the ventricle. Phosphorylation of 4EBP1/2, but not S6, was responsive to quiescence induction in cultured embryonic NSCs. Further, inhibition of p-4EBP1/2, but not p-S6, was sufficient to induce quiescence. Collectively, this work offers new insight into the regulation of quiescence entry in embryonic NSCs and, thereby, correct patterning of the adult brain. These data suggest unique biological functions of specific posttranslational modifications and indicate that the preferential inhibition of such modifications may be a useful therapeutic approach in neurodevelopmental diseases where NSC numbers, proliferation, and differentiation are altered.

Introduction

The ventricular-subventricular zone (V-SVZ) is the largest neural stem cell (NSC) niche in the postnatal mammalian brain and cells from this niche produce multiple subtypes of neurons and glia (Alvarez-Buylla & García-Verdugo, 2002; Bond et al., 2021; Chaker et al., 2016; David-Bercholz et al., 2021; Delgado et al., 2021; Doetsch et al., 1997; Ihrie & Álvarez-Buylla, 2011; Merkle et al., 2004; Obernier & Alvarez-Buylla, 2019; Radecki & Samanta, 2022; Young et al., 2007). Postnatal adult NSCs, also termed B1 cells, are derived from a subpopulation of embryonic NSCs, termed pre-B1 cells, that enter a transient quiescence during mid- to late- neurogenesis, with the cell cycle slowing down beginning at embryonic day 13.5 and being completed by embryonic day 15.5. These cells remain quiescent until reactivation in early adulthood (postnatal days 21 – 28) (Fuentealba et al., 2015; Furutachi et al., 2015). Disruptions to either the cycling kinetics or total number of quiescent NSC populations in the embryo alter postnatal neurogenesis in both the V-SVZ and the dentate gyrus, the second major neurogenic niche (Berg et al., 2019; Bond et al., 2021; Hu et al., 2017; Kokovay et al., 2012; D. Y. Wang et al., 2020). While prior work has established that the regenerative capacity of the adult brain is directly related to pre-B1 cells' transient quiescence entry, little is known about the dynamics and regulation of this essential process.

The mechanistic/mammalian target of rapamycin (mTOR) kinase is a principal regulator of cell growth (Laplante & Sabatini, 2012; G. Y. Liu & Sabatini, 2020) that has been shown to regulate the quiescence of other stem cell populations, including in postnatal NSCs (Cho & Hwang, 2012; Nieto-González et al., 2019; Rodgers et al., 2014; Rossi et al., 2021; Sousa-Nunes et al., 2011). However, this potential relationship has not yet been explored in embryonic NSCs. The two primary downstream effectors of mTOR, phosphorylated ribosomal S6 kinase (p-S6) and phosphorylated 4E-binding proteins (p-4EBP1/2), have not been systematically characterized together in embryonic NSCs throughout neurogenesis or in the context of quiescence. Canonically, p-S6 regulates cell size and growth through its

function in the ribosome, while p-4EBP1/2 is involved in cap-dependent mRNA translation (Gingras et al., 1999; Magnuson et al., 2012; Montagne et al., 1999; Ruvinsky & Meyuhas, 2006). However, in many studies, either p-S6 is used as the sole readout of mTOR activity, or the two proteins are used interchangeably. A growing body of evidence suggests that these two proteins have distinct, non-compensatory biological functions that are triggered by phosphorylation (Magnuson et al., 2012). Specifically, in postnatal NSCs, p-4EBP1/2 has been shown to regulate selective translation and regulation of self-renewal (Hartman et al., 2013). In glioblastoma cell lines, only p-4EBP1/2 was shown to correlate with a cell's entry to or exit from the cell cycle (Fan et al., 2017, 2018).

Additionally, p-4EBP1/2 and p-S6 can behave independently in response to different ligands binding the upstream receptors that can activate this signaling pathway, such as insulin, growth factors, or amino acids (Sparta et al., 2021). Establishing the differences in activity and function between p-S6 and p-4EBP1/2 in embryonic NSCs may have direct relevance for patients with disorders of dysregulated mTOR signaling for whom mTOR inhibitors are often prescribed (Cavalheiro et al., 2021; Ebrahimi-Fakhari et al., 2021; Franz, 2011; Karalis & Bateup, 2021; Overwater et al., 2019). Three generations of mTOR inhibitors currently exist and have differing potencies and relative abilities to inhibit p-S6 and p-4EBP1/2. First generation rapamycin and analog drugs, termed "rapalogs," have repeatedly been shown to have a greater effect on p-S6 than p-4EBP1/2 and on mTOR complex 1 (mTORC1) than complex 2 (mTORC2) (Choi et al., 1996; Fan et al., 2018). Second generation Tork inhibitors were designed to have improved potency against mTORC2 (Feldman et al., 2009), while third generation inhibitors, including RapaLink-1, were designed to have improved potency against p-4EBP1/2 (Rodrik-Outmezguine et al., 2016). This array of inhibitors offers an opportunity to separate the biological effects of p-S6 and p-4EBP1/2 in embryonic NSCs, where they have been untested, and their potential contributions to quiescence.

Here, the signaling patterns of mTOR targets in embryonic NSCs of the V-SVZ and their potential involvement in pre-B1 cell quiescence were investigated by adapting an established *in vitro* model of reversible quiescence to prenatal cells and quantifying functional effects of modulating downstream targets of mTORC1. p-4EBP1/2 and p-S6 were found to be expressed independently, not coordinately, in distinct populations of NSCs in the embryonic brain. The proliferative ability of an embryonic NSC was dependent upon phosphorylation of 4EBP1/2, as decreases in p-4EBP1/2, but not S6, were sufficient to induce quiescence. These results suggest mTOR-dependent phosphorylation of 4EBP1/2 is a key regulatory step in quiescence entry of embryonic pre-B1 NSCs and thus establishment of the postnatal stem cell niche.

Materials and Methods

Animals: All procedures involving animals were performed in accordance with animal health, safety, and wellness protocols outlined by both institutional (Institutional Animal Care and Use Committee) and national (National Institute of Health) governing bodies. Wild type C57 Black 6 mice were obtained from Charles River Laboratories. To collect embryos for cells, timed pregnant embryonic day 15.5 (E15.5) dams were euthanized via Avertin overdose and dissected. The embryos were collected for culture generation as described in the following sections. To collect embryos for tissue sections, timed pregnant E13.5, E15.5, and E17.5 dams were euthanized via Avertin overdose and transcardially perfused with 0.9% saline followed by 4% paraformaldehyde solution diluted in 0.2M phosphate buffer. Dissected embryos were processed further for imaging as described in the following sections.

iDISCO+ Tissue Clearing: Whole E13.5 embryos were processed, stained, and cleared according to the immunolabeling-enabled three-dimensional imaging of solvent-cleared organs (iDISCO+) protocol described in Renier et al., 2014. Briefly, following perfusion of the pregnant dam, the embryos were drop fixed in 4% paraformaldehyde overnight at 4°C, and stored in PBS containing 0.1% sodium azide until staining. The embryos were dehydrated in six methanol washes (20%, 40%, 60%, 80%, and 100% at room temperature and a 100% wash chilled to 4°C), stored overnight in 66% dichloromethane in methanol at 4°C, washed twice with methanol (100%) at room temperature, and bleached overnight with 5% hydrogen peroxide in methanol at 4°C. The samples were rehydrated through washes in methanol (80%, 60%, 40%, 20%), 1X PBS, and two washes in buffer containing PBS and 0.2% TritonX-100 – one at room temperature and one overnight at 4°C. All washes, except those that lasted overnight, were 1 hour. Samples were incubated for 12 hours at 37°C with a permeabilization solution containing 10% PBS/0.2% TritonX-100/20% DMSO/2.3% glycine and incubated for 12 hours at 37°C with blocking solution containing 10% PBS/0.2% TritonX-100/6% normal donkey serum/10% DMSO. The samples were

incubated for 24 hours with primary antibodies in buffer containing 10% PBS/0.2% Tween-20/0.1% 10 mg/mL Heparin/5% DMSO/3% normal donkey serum at 37°C, washed for 24 hours in buffer containing 10% PBS/0.2% Tween-20/0.1% 10 mg/mL Heparin at 37°C, incubated for 24 hours with Alexa Fluor secondary antibodies (Thermo Fisher Scientific) in buffer containing 10% PBS/0.2% Tween-20/0.1% 10 mg/mL Heparin/3% normal donkey serum at 37°C, and washed for an additional 24 hours in buffer containing 10% PBS/0.2% Tween-20/0.1% 10 mg/mL Heparin at 37°C. Antibodies are listed in Table 2. The samples were dehydrated through six hour-long washes in methanol (20%, 40%, 60%, 80%, 100%, 100%), incubated for 3 hours in 66% dichloromethane in methanol, washed twice in dichloromethane for 15 minutes, and cleared and stored in dibenzyl ether until imaging at 4X and 15X via SmartSPIM (LifeCanvas Technologies) light sheet fluorescence microscope. Imaris Software version 9.5.1 was used for image and video reconstruction.

Immunostaining of Mouse Brains: The heads were removed from E13.5, E15.5, and E17.5 embryos, drop fixed in 4% paraformaldehyde 2 hours (for 10 µm thick sections) or overnight (for 50 µm thick sections) at 4°C, and then sunk in 30% sucrose solution. Fixed heads were embedded into optimal cutting temperature compound (OCT) (Tissue-Tek, Sakura, 4583) before cryosectioning and mounting on Color Frost Plus microscope slides (Thermo Fisher Scientific, 12-550-16). Slides with OCT-embedded embryonic brain slices were removed from the freezer and allowed to acclimate to room temperature for 20 minutes in the chemical hood. Slides were washed three times in 1X PBS for 5 minutes, incubated in blocking solution containing PBS/1% normal donkey serum/1% BSA/0.1% Triton X-100 for 30 minutes at room temperature. Primary antibodies and primary-secondary antibody conjugates were applied to the slides overnight at 4°C. Antibodies are listed in Table 2. Slides were washed again three times in 1X PBS for 5 minutes and Alexa Fluor secondary antibodies (Thermo Fisher Scientific) were applied to the slides for approximately 1 hour at room temperature. Slides were washed one time with 1X PBS for 5 minutes. 4□,6-diamidino-2-phenylindole (DAPI) (diluted 1:10,000 in 1X PBS) was applied to the slides for

20 minutes at room temperature. The slides were washed 2 final times in 1X PBS for 5 minutes and rinsed with ddH20. Mowiol or Fluoromount-G (Electron Microscopy Sciences, 1798425) were used to mount coverslips (Fisher Scientific, 12-544-18P) and the slides were allowed to dry overnight. Slides were imaged on an LSM 710 Confocal Microscope (Zeiss) at specified magnifications and z-stacks at the Vanderbilt Cell Imaging Shared Resource and Zen Blue software (Zeiss) was used for image acquisition and reconstruction.

Human Induced Pluripotent Stem Cell (hiPSC) Cell Culture: Two hiPSC lines (1) GM25256s from the Coriell Institute and (2) 77s from the Sahin lab (Sundberg et al., 2018) were cultured as previously described (Armstrong et al., 2017; Chalkley et al., 2022; Snow et al., 2020). In brief, iPSCs were grown as colonies on Matrigel (Corning, 354277) coated 6 well plates in mTeSR1 medium (StemCell Tech, 85850) at 37°C and 5% CO_2. Culture media was replaced daily, and the cells were passaged with ReLSR (StemCell Tech, 05872) upon reaching confluency.

Cortical Neurosphere Culture: iPSCs at 70% confluence were incubated with Accutase (Stem Cell Technologies, 07920) for 5 minutes at 37°C to dissociate cells. Cells were pelleted via centrifugation for 5 minutes at room temperature at 300 x *g*. 3 million cells were added to one well of an Aggrewell™800 (StemCell Tech, 34815) with neural induction media, containing 1:1 mixture DMEM/F12 GlutaMAX (Gibco, 10565-018) and Neurobasal (Gibco, 21103049), 0.5X N2 (Gibco, 17502048), 0.5X B27 with vitamin A (17504044), 2.5 µg/mL insulin (Life Technologies, 12585014), 0.75X Glutamax (Gibco, 35050061), 50 µM nonessential amino acids (Sigma, M7145), 50 µM 2-mercaptoethanol (Sigma, M6250), 50 U/mL penicillin-streptomycin (Gibco, 15140122), 10 µM SB431542 (Cayman Chemical, 13031) and 100 nM LDN-193189 (Tocris, 6053). Cells were allowed to aggregate overnight into a sphere while maintained at 37°C and 5% CO_2. Neural induction media was replaced daily for 10 days. After 24

hours in culture, the neurospheres were transferred into well plates and maintained in suspension on an orbital shaker (95 rpm).

Immunostaining of Neurospheres: All neurospheres were fixed by incubation in 4% paraformaldehyde for 15 minutes at 4°C. Fixed samples were blocked with blocking buffer containing PBS/1% normal donkey serum/1% BSA/0.1% Triton X-100 for 1 hour at room temperature. Primary antibodies were diluted in blocking buffer and then incubated overnight at 4°C. Alexa Fluor secondary antibodies (Thermo Fisher Scientific) were diluted in blocking buffer and then incubated 1 hour at room temperature in the dark. Antibodies are listed in Table 2. Hoechst (diluted 1:10,000 in 1X PBS) was applied to the slides for 20 minutes at room temperature. Images were acquired using a Prime 95B camera mounted on a Nikon spinning disk confocal microscope using a Plan Apo Lambda 20x objective lens at the Vanderbilt Nikon Center of Excellence. The software used for image acquisition and reconstruction were NIS-Elements Viewer (Nikon) and ImageJ (FIJI).

Cell Pellet Preparation: Cultured cells were dissociated using Accutase and pelleted via centrifugation for 5 minutes at room temperature at 100 x *g* prior to fixation with 1.6% paraformaldehyde for 15 minutes, washed with 1x PBS, and re-pelleted via centrifugation for 5 minutes at room temperature at 100 x *g*. The supernatant was removed and replaced with 70% ethanol. The pellet was then paraffin embedded and prepared as 5-7 µm sections.

Quantification of *ex vivo* Mouse Imaging Data: A custom Stardist 3D nuclear segmentation model was trained using 16 expert annotated cropped regions of interest from the dataset using the protocol described at https://github.com/stardist/stardist. Nuclear segmentation model was applied to each image in dataset followed by 3D pixel expansion to segment probable cell bodies. Marker mean intensity was measured and recorded for each nucleus, cytoplasm, and cell body (nucleus + cytoplasm). For each

measured marker, cells were scored as positive or negative by thresholding. Thresholds were set and confirmed per staining batch by two independent viewers (LCG and AAB).

Quantification of *in vitro* Human Imaging Data: A custom Stardist 2D nuclear segmentation model was trained using 18 expert annotated cropped regions of interest from the dataset using the protocol described at https://github.com/stardist/stardist. The model was applied to each image in the dataset followed by 2D pixel expansion to segment probable cell bodies. Marker mean intensity was measured and recorded for each nucleus, cytoplasm, and cell body (nucleus + cytoplasm). For each measured marker, cells were scored as positive or negative by thresholding. Thresholds were set and confirmed per staining batch by two independent viewers (LCG and AAB).

Primary Cell Cultures: Mouse embryos were collected at E15.5 from timed pregnant dams. To obtain stem cell cultures from the developing V-SVZ, a "top-down" dissection approach was employed. Briefly, the heads were separated from the body, the two brain hemispheres were pulled back to either side to reveal the developing cortex which was collected as dorsal NSCs. The developing ganglionic eminences were collected as ventral NSCs. The collected tissue was minced and incubated at 37°C, 5% CO2 with 0.25% trypsin-EDTA solution for 20 minutes while rocking. The tissue was then gently dissociated via trituration with a pipette and the cells were cultured and maintained in media specific to embryonic neural stem cells as described in Moghadam et al., 2018: Neurobasal media (ThermoFisher, 21103049); 1X B27 supplement without vitamin A (ThermoFisher, 12587010); 20 ng/mL mouse epidermal growth factor (ThermoFisher, 53003018); 10 ng/mL mouse basic fibroblast growth factor (ThermoFisher, PMG0035); 1 U/mL heparin (Sigma, 9041-08-01); 1X GlutaMax (ThermoFisher, 35050061); 1X modified Eagle's medium non-essential amino acids (11140050); 0.1 mM β-mercaptoethanol; 10 µg/mL gentamicin. Cells were fed every 2-3 days and passaged upon reaching confluence.

Quiescence Induction: To induce quiescence, embryonic NSC media was prepared as above without epidermal growth factor and with the addition of 50 ng/mL mouse bone morphogenetic protein 4 (R&D Systems, 5020-BP-010, stock dissolved in 4 mM hydrochloric acid with 0.1% BSA). Cells were fed every 2-3 days.

Pharmacological modulators: mTOR inhibitors were added to culture media at concentrations listed in text and figure legends. Initial dissolutions of inhibitors were in DMSO, as specified by manufacturers' instructions, and subsequent dilutions of concentrated stocks were in PBS.

Table 1

Reagent	Vendor	Catalog Number
4EGI-1	Selleck Chem	S7369
RapaLink-1	Cell Signaling Technologies	88626S
Rapamycin	Tocris	1292
Torin1	Selleck Chem	S2827
Torin2	Selleck Chem	S2817
Torkinib (PP242)	Selleck Chem	S2218

Fluorescence flow cytometry: Cultured NSCs were collected for flow cytometry as previously described (Irish et al., 2010; Rushing et al., 2019). Briefly, cultures were gently dissociated for 7-10 minutes using Accutase at 37°C, pelleted by centrifuging for 5 minutes at room temperature at 100 x *g*, resuspended in 1 mL of the original spent media in 5 mL round bottom tubes (352052; Corning), and allowed to rest at 37°C for 1 hour and 25 minutes. Alexa Fluor 700-succinimidyl ester (Invitrogen, A20010) was added to the media at 37°C for 5 minutes to label non-intact cells. Samples that were to be live stained were then centrifuged for 5 minutes at room temperature at 100 x *g*, incubated with anti-VCAM1 antibody for 15 minutes at room temperature, rinsed with 1X PBS, and centrifuged again for 5 minutes at room temperature at 100 x *g*. All samples were then fixed with 1.6% paraformaldehyde, permeabilized with 70% ice cold ethanol, and stored at -20°C until staining. On the day of staining, samples were washed 2X

with PBS and spun at 800 x *g* for 5 minutes at room temperature. Cells were stained with a cocktail of antibodies against intracellular antigens diluted in PBS/1% BSA for 30-60 minutes at room temperature. Samples were washed with PBS and spun at 800 x *g* for 5 minutes at room temperature. Samples were analyzed on either a Fortessa 4-laser or 5-laser instrument. Beads (Invitrogen, A10513) stained with a single fluorophore and unstained cells from the same cell line and treatment conditions were used for compensation and sizing controls. Gating was performed to isolate live, intact, single cells. Signaling values for each antigen were determined as both (1) the arcsinh transformed and (2) fold change of each sample compared to the column minimum for each antigen. The arcsinh scale used has been previously described (Irish et al., 2010; Rushing et al., 2019). On the arcsinh scale, a difference in 0.4 corresponds to a nearly 2-fold difference in total protein. All analyses were performed in Cytobank.

Cell cycle analysis: Cultured cells were dissociated for 7-10 minutes using Accutase at 37°C, pelleted by centrifuging for 5 minutes at room temperature at 100 x *g*, resuspended in the original spent media in 5 mL round bottom tubes and incubated for 5 minutes with AlexaFluor700-succinimidyl ester to label non-intact cells. Cells were fixed with 1.6% paraformaldehyde, permeabilized with 70% ice cold ethanol, and stored at -20°C until staining. On the day of staining, samples were washed with PBS and spun at 800 x *g* for 5 minutes at room temperature twice. Cell pellets were resuspended in 1.5 µM Hoechst 33342 (Cell Signaling Technology, 4082) and incubated for 1 hour at 37°C and vortexed and every 15 minutes during incubation. Samples were analyzed on a BD LSRII 5-laser instrument. Cells in each phase of the cell cycle were determined via gating of live, intact, single cells. All analyses were performed in Cytobank.

Quantification and statistical analysis: The quantification methods used and statistical tests performed are detailed in each figure and figure legend. GraphPad Prism 9 was used to perform all analyses.

Data Availability Statement: All flow cytometry data will be made publicly available on FlowRepository upon publication (Spidlen et al., 2012).

299

300

301

302

303 **Antibodies:**

304 Table 2

Antibody	Species	Clone	Catalog Number	Vendor	Dilution
CD106 (VCAM1) conjugated to BV605	Rat	429	745193	BD Biosciences	1:200
Ki67	Rat	Sola15	14-5698-82	Thermo Fisher	1:200
Ki67 conjugated to PerCP-Cy5.5	Mouse	B56	561284	BD Biosciences	1:40
p-4EBP1/2 T37/46	Rabbit	236B4	2855	Cell Signaling Technologies	1:800 (slides); 1:400 (iDISCO+)
p-4EBP1/2 T37/46 conjugated to Ax647	Rabbit	236B4	5123S	Cell Signaling Technologies	1:100 (FC), 1:200 (IHC)
p-S6 S235/236 conjugated to Pacific Blue	Rabbit	D57.2.2E	8520S	Cell Signaling Technologies	1:100
p-S6 S240/244	Rabbit	D68F8	5364	Cell Signaling Technologies	1:800 (slides); 1:400 (iDISCO+)
p-S6 S240/244 conjugated to Ax488	Rabbit	D68F8	5018S	Cell Signaling Technologies	1:400 (Flow cytometry), 1:400) (IHC)
p-STAT3 S727 conjugated to PE	Mouse	49P-STAT3	558557	BD Biosciences	1:15
p-Vimentin S55	Mouse	4A4	D076-3	MBL	1:1000
Sox2	Rat	Btce	14-9811-82	Invitrogen	1:100
Sox2 conjugated to PerCP-Cy5.5	Mouse	O30-678	561506	BD Biosciences	1:400
Tbr2	Chicken	Polyclonal	AB15894	Millipore	1:250

305

306

307

308

309

310

Experimental Design

Mouse Experiments: The control groups for each experiment are listed in each figure legend. Both male and female embryos were used for immunohistochemistry experiments. Each embryo counted as a unique biological replicate (N=1). Embryos used in experiments presented here span at least two litters from each timepoint. Cultures were generated by pooling tissue collected from the indicated region from all the embryos (both male and female) from 1 or 2 timed pregnant dams, with an average litter size of 7. Cultures were grown up for one passage before cryopreservation. Each thawed cryovial counted as a unique biological replicate (N=1). Cultures used in experiments presented here represent three independent pregnant dam dissections and culture generations. Cultures treated with BMP4 were compared to matched cultures from the same cryovial that were not exposed to BMP4. Cultures treated with a pharmacological inhibitor were compared to matched cultures from the same cryovial treated with vehicle (1X PBS).

Human Cells: Neurospheres were differentiated from two unique wild type induced pluripotent stem cell lines. Each differentiation counted as a unique biological replicate (N=1). Individual neurospheres from each biological replicate were considered technical replicates.

Statistical Analysis: Unless otherwise indicated, all experiments had an N of at least 3. Exact Ns (separate biological replicates) are listed in the figure legends for each experiment. D'Agostino and Pearson K-squared tests were performed on each dataset to determine departure from normality. If a dataset failed to reach normality (p value < 0.05) or did not have enough replicates to perform the D'Agostino test ($N < 8$), then a nonparametric Mann-Whitney U test was performed. If the dataset reached normality (D'Agostino test p value > 0.05), a parametric student's t-test was performed. Whether the test was paired or unpaired is indicated in the figure legends for each comparison. P values

for each comparison are listed in the figure legends. GraphPad Prism 9 was used to perform all statistical analyses and generate plots.

Results

High levels of p-4EBP1/2, but not p-S6, are present in embryonic NSCs at the ventricle.

To visualize levels of mTORC1 signaling prior to the genesis of pre-B1 cells, whole brains from embryonic day 13.5 mice were processed, cleared, and stained for p-S6 S240/244 and p-4EBP1/2 T37/46. p-S6 S240/244 was distributed in multiple cell layers of both the developing cortex and ganglionic eminences (Fig 1A). In contrast, p-4EBP1/2 T37/46 was primarily present in cell bodies lining the apical ventricular surface of developing cortex and was not abundant in cells that were more distant from the ventricle. In the lateral and medial ganglionic eminences, p-4EBP1/2 was similarly enriched at the ventricular surface and was also present in some cells deeper within the tissue (Fig 1B; full brain videos for p-S6 and p-4EBP1/2 in Extended Fig 1-1). To further investigate these patterns throughout neural development and the genesis of pre-B1 cells, coronal sections of embryonic day 13.5, 15.5, and 17.5 mouse brain were co-stained for both readouts of mTORC1 activity (Fig 1C). At all developmental ages measured, the two phosphorylated proteins were largely found in distinct cells. p-4EBP1/2 labeling was limited to cells lining the ventricular surface, many of which appeared to be actively undergoing mitosis (yellow arrows in Fig 1C). At E13.5 and 15.5, p-S6 was not found in cells lining the ventricular surface but was abundant in the subventricular zone and intermediate zones. At E17.5, p-S6 was observed in cells contacting the ventricular surface. The two phosphorylated proteins were rarely found in the same cell (E13: average 2.7% of counted cells [N=3], E15: average 0.52% of counted cells [N=4], E17: average 0.1% of counted cells [N=3]). The frequency of p-4EBP1/2-positive cells decreased with gestational age, from an average of 4.10% of cells per field at E13.5 to 0.17% at E17.5, while levels of p-S6 expression increased from 37.85% at E13.5 to 53.78% at E17.5.

Co-staining with Ki67, a marker of cycling cells, revealed that p-4EBP1/2 positive cells were often dividing: 80.97% of cells positive for p-4EBP1/2 at E13.5 were doubly positive for Ki67, 68.44% at E15.5, and 33.33% at E17.5; though Ki67 expression also decreased with age (27.02% of total cells at E13.5,

18.01% at E15.5, 2.54% at E17.5), consistent with prior reports (Hu et al., 2017) and the general decrease in neurogenesis at this stage (Fuentealba et al., 2015; Furutachi et al., 2015). p-S6 positive cells variably expressed Ki67 (31.26% of cells positive for p-S6 at E13.5, 27.93% at E15.5, 3.29% at E17.5). Additional Ki67 staining in the developing V-SVZ at E13.5 from cleared brain is shown in Extended Fig 1-1. To assign mTOR activity more precisely to radial glia and transit amplifying cells, tissues were co-stained for p-S6 S240/244, p-4EBP1/2 T37/46, and the transcription factor t-box brain protein 2 (Tbr2), which distinguishes the transit-amplifying progeny of cortical radial glia (Englund et al., 2005) (Fig 1E). Cells expressing Tbr2 were more likely to express p-S6 than p-4EBP1/2 at both E13.5 (12.99% Tbr2/p-S6 co-positive cells versus 0.65% Tbr2/p-4EBP1/2 co-positive cells) and E15.5 (34.72% Tbr2/p-S6 co-positive cells versus 2.26% Tbr2/p-4EBP1/2 co-positive cells).

As cells positive for p-4EBP1/2 were often co-positive for Ki67 and appeared to be actively dividing, this suggested that cells with low expression of p-4EBP1/2 could be pre-B1 cells, which have been reported to enter quiescence during prenatal development. Lineage tracing studies have indicated that pre-B1 cells begin entering quiescence as early as E13.5, with most completing quiescence entry by E15.5 (Fuentealba et al., 2015; Furutachi et al., 2015). E15.5 brains were co-stained with p-S6 S240/244, p-4EBP1/2 T37/46, and vascular cell adhesion molecule 1 (VCAM1), a protein required for the maintenance of the radial glia stem cell population and entry into quiescence (Hu et al., 2017; Kokovay et al., 2012; D. Y. Wang et al., 2020) (Fig 1F). VCAM1 was found infrequently in the developing cortex, but was more abundant in the ganglionic eminences, consistent with previously published findings (Hu et al., 2017) (Fig 1D, 20x). At E15.5, VCAM1 was expressed exclusively by cells at the ventricular surface and did not overlap with p-S6. Line scan analysis along the apical ventricular surface showed that cells positive for p-4EBP1/2 and VCAM1 were largely exclusive of each other (Figure 1D). In pixels negative for p-4EBP1/2, the average VCAM1 intensity was double that in pixels positive for p-4EBP1/2 (4.22 versus 2.04, N = 3).

To determine if similar patterns of p-4EBP1/2 / p-S6 dual abundance might be present in human neural progenitors, neurospheres were differentiated from two separate wild type human induced pluripotent stem cell lines (Sundberg et al., 2018). After 10 days in culture, neurospheres were collected and were co-stained with p-S6 S240/244, p-4EBP1/2 T37/46, and Ki67 (Fig 1G). As was observed in the mouse, p-S6 was more abundantly expressed than p-4EBP1/2 (21.78% of total cells positive for p-S6 versus 4.55% positive for p-4EBP1/2, N = 5 neurospheres) and cells positive for p-4EBP1/2 were often actively undergoing division and doubly positive for Ki67 (61.72% of p-4EBP1/2 positive cells). Similar to the pattern observed in the mouse, only a small percentage of cells (4.00% of total cells) were positive for both p-S6 and p-4EBP1/2.

Exposure to BMP4 induces quiescence in embryonic NSCs *in vitro*.

To determine how mTOR activity responds to changes in cellular proliferation and assess whether cells entering quiescence decrease levels of p-4EBP1/2, an *in vitro* model of quiescence was developed and validated. The role of bone morphogenetic protein 4 (BMP4) in directing differentiation and maintenance of stem cells in the V-SVZ and dentate gyrus has been extensively described (Li et al., 1998; Mira et al., 2010). BMP4 has been reported to induce a reversible quiescence *in vitro* in various stem cell populations within 72 hours, including postnatal neural stem cells (Knobloch et al., 2017; Mira et al., 2010; Rossi et al., 2021), but has not been tested in prenatal NSCs.

To test its use in prenatal NSC populations, neural stem cells dissected from the developing dorsal V-SVZ at embryonic day 15.5 were exposed to BMP4 with simultaneous withdrawal of EGF but maintenance of basic fibroblast growth factor (bFGF-2), and markers of cell proliferation and quiescence were quantified using fluorescence microscopy and flow cytometry. After 24 hours in media containing BMP4 and bFGF-2, levels of the proliferation marker Ki67 had significantly decreased compared to cells grown in control media containing bFGF-2 and epidermal growth factor (EGF) (Fig 2A), with a further decrease seen by 72 hours and persisting with additional time in BMP4 culture media (time course of

quiescence entry shown in Extended Fig 2-1). Following extended incubation with BMP4/FGF-2 media for 6 days, Ki67 and p-vimentin levels both remained decreased compared to control (Fig 2B). BMP4-mediated decreases in Ki67 were reversible, as re-exposure to media containing EGF and lacking BMP4 rescued levels of Ki67 (Extended Fig 2-2). Within 24 hours of exposure to BMP4/FGF-2 media, levels of VCAM1 also began to rise compared to control cells and remained high at 72 hours (Fig 2C). To further verify that BMP4 was having the desired effect, the percentage of cells in each stage of the cell cycle was determined following 24 hours of exposure to BMP4. Cells grown in media containing BMP4/FGF-2 had an increased percentage of cells in the G0/G1 phase of the cell cycle compared to cells grown in media containing EGF/FGF-2 (averages of 80.83% vs 58.08%, N=9), and had a decreased percentage of cells in both the S (7.03% vs. 21.70%) and G2/M (8.98% vs 17.31%) phases of the cycle compared to control cells (Fig 2D; gates used to determine percent of cells in each phase of the cell cycle shown in Extended Fig 2-3).

BMP4 has also been shown to direct NSCs into neuronal or astrocytic lineages depending on the time of expression (Katada et al., 2021); these effects that are directly antagonized and suppressed by EGF and FGF-2 to maintain stemness and self-renewal capacities (Lillien & Raphael, 2000; Sun et al., 2011). To ensure that the removal of EGF and exposure to BMP4 did not differentiation as reported for media containing only BMP4 without FGF-2, levels of Sox2, a transcription factor expressed by neural stem and progenitor cells, but not transit amplifying cells, were measured following acute (72 hours, Fig 2E) and prolonged (6 days, Fig 2F) exposure to BMP4. At 72 hours of BMP4 exposure, levels of Sox2 remained unchanged compared to cells grown in EGF/FGF-2 media. At 6 days in culture with BMP4, per-cell Sox2 expression remained high and comparable to cells grown in EGF/FGF-2 media. Further, cells cultured with BMP4 did not begin to express markers of differentiation, including TUJ1 or GFAP (Extended Fig 2-3). Taken together, these data indicate that consistent with published models, BMP4 in

combination with FGF-2 efficiently induces reversible quiescence in embryonic NSCs *in vitro* within 24 hours without inducing differentiation.

p-4EBP1/2 signaling decreases in embryonic NSCs following quiescence induction.

To investigate whether low levels of p-4EBP1/2 were directly correlated with quiescence, neural stem cells dissected from the developing cortex at embryonic day 15.5 were cultured in media containing BMP4 and FGF-2 for acute (24 hours) or extended (72 hours) time periods and readouts of the mTOR pathway were measured. Two different phosphorylated sites on S6 were measured: S235/236, a residue phosphorylated by both the mTOR and MAPK/ERK pathways, and S240/244, a residue exclusively phosphorylated by the mTOR pathway (Magnuson et al., 2012; Roux et al., 2007). At both 24 and 72 hours in BMP4/FGF-2 media, neither of these readouts showed significant change relative to EGF/FGF-2 media (Figs 3B and Fig 3C), a pattern that was persisted after further prolonged exposure to BMP4/FGF-2 media (6 days, Fig 3D). In contrast, after 24 hours in media containing BMP4, levels of p-4EBP1/2 decreased compared to controls (Fig 3E), with a further decrease seen after 72 hours. To determine whether the decrease in p-4EBP1/2 remained after prolonged exposure to BMP4 and corresponded to a decrease in proliferation, cells were cultured for 6 days and co-stained for KI67 and p-4EBP1/2 (Fig 3F). Levels of both Ki67 and p-4EBP1/2 decreased upon exposure to BMP4, compared to cells grown in EGF/FGF-2 media. At both 24 and 72 hours of BMP4 exposure, levels of an additional mTOR target, p-STAT3 S727 (Dodd et al., 2015; Yokogami et al., 2000), also decreased compared to the EGF/FGF-2 media condition (Fig 3A).

Decreases in mTOR-dependent phosphorylation of S6 are not sufficient to induce quiescence.

Next, inhibition of these downstream components of mTOR signaling was tested for sufficiency in inducing quiescence. Rapamycin, a first generation mTOR inhibitor, has frequently been reported to inhibit the phosphorylation of S6 more effectively than that of 4EBP1/2 due to its specific binding

location on mTOR (Choi et al., 1996; Fan et al., 2018). In cultures of embryonic day 15.5 NSCs, 30 nM of Rapamycin decreased levels of p-S6, but did not affect levels of p-4EBP1/2 after 4 hours (Fig 4A). After 24 hours in culture, p-S6 levels recovered and were not significantly different from vehicle treated levels (Extended Fig 4-1). Torkinib (PP242) is a second generation, dual mTORC1 and mTORC2 inhibitor that has been reported to inhibit phosphorylation of both S6 and 4EBP1/2 (Feldman et al., 2009), and was tested here in a dose response series ranging from 12.5 nM to 400 nM of Torkinib (Fig 4A). At all concentrations tested, 4-hour treatment with Torkinib decreased phosphorylation of S6 at both the mTOR-dependent S240/244 and alternate S235/236 residues. However, phosphorylation of 4EBP1/2 remained unaffected at all concentrations tested. Following acute (4 hour) and extended (24 hour) treatment with 400 nM Torkinib, levels of p-STAT3 S727 similarly did not decrease (Fig 4B). Additional second generation mTOR inhibitors and inhibitors of specific cap-dependent translation components were tested for their ability to decrease levels of p-4EBP1/2 in cultures; however, none had this ability (Extended Fig 4-1). Torkinib was therefore used as an S6-selective inhibitor to determine whether inhibition of phosphorylation of S6, but not 4EBP1/2, would be sufficient to induce quiescence. While levels of p-S6 S235/236 (Fig 4C) and p-S6 S240/244 (Fig 4D) initially decreased following 4 hour treatment with Torkinib, by 24 hours, both proteins had overcome the inhibition and were not different compared to vehicle treated cells. Phosphorylation of 4EBP1/2 was unaffected by treatment with Torkinib at both 4 and 24 hours (Fig 4E). Neither length of treatment affected levels of Ki67 (Fig 4F). While there was a small increase in the percentage of cells in G0/G1 with Torkinib treatment compared to vehicle after 24 hours of treatment (averages of 75.03% Torkinib vs 72.67% vehicle, N=9), there was not a significant decrease in the percent of cells in the S (7.73% vs 7.90%) or G2/M phases (16.01% vs. 15.06%) of the cycle with treatment (Fig 4G). Taken together, these data indicated inhibition of S6 phosphorylation alone was not sufficient to induce quiescence. Given that levels of p-4EBP1/2

476 decreased upon entry into quiescence, inhibition of p-4EBP1/2 was next tested for sufficiency to induce
477 quiescence.

478 **Decreases in mTOR-dependent phosphorylation of 4EBP1/2 are sufficient to induce quiescence.**

479 RapaLink-1, a third generation mTOR inhibitor synthesized from Rapamycin and an ATP-
480 competitive inhibitor of mTOR, MLN0128 (Rodrik-Outmezguine et al., 2016), has previously been shown
481 to inhibit phosphorylation of 4EBP1/2 in mouse brain tissue (Zhang et al., 2022). Following 24 and 72
482 hours of treatment with 10 nM RapaLink, E15.5 NSCs were analyzed for readouts of the mTOR pathway.
483 Levels of p-STAT3 S727 were unaffected compared to vehicle at 24 hours, but after 72 hours of
484 treatment with RapaLink, the values were slightly decreased compared to vehicle (Fig 5A). Levels of both
485 p-S6 S235/236 (Fig 5B) and p-S6 S240/244 (Fig 5C) decreased following 24 hours of treatment with
486 RapaLink and stayed low compared to vehicle after 72 hours of treatment, contrasting with the transient
487 effects of Torkinib. Levels of p-4EBP1/2 decreased compared to vehicle following 24 hours of treatment
488 with RapaLink and remained decreased after 72 hours (Fig 5D). After 24 hours of treatment with
489 RapaLink, levels of Ki67 were significantly decreased compared to vehicle and remained so at 72 hours
490 (Fig 5E). After 24 hours of treatment, RapaLink treated cells had an increased percentage of cells in the
491 G0/G1 phases of the cell cycle (averages of 78.63% with RapaLink vs. 67.42% with vehicle, N=7) and
492 decreased percentages of cells in the S (12.27% vs. 18.71%) and G2/M phases (5.98% vs. 11.50%) of the
493 cell cycle compared to vehicle treated cells. Taken together, these data indicate that inhibition of
494 4EBP1/2 is sufficient to induce quiescence in cultured embryonic NSCs.

495 **Quiescence entry and mTOR response do not differ by dorsoventral position.**

496 Prior studies of postnatal cells found that NSCs from the ventral V-SVZ exhibited higher per-cell
497 phosphorylation of mTORC1 targets than their dorsal counterparts (Rushing et al., 2019). To determine
498 whether embryonic cells also had differential mTOR signaling based on cellular positioning, NSCs from

the developing cortex (dorsal NSCs) and cells from the ganglionic eminences (ventral NSCs) were cultured separately and the various mTOR readouts were assessed before and after quiescence induction. In cultures maintained in media containing EGF/FGF-2, no uniform differences between dorsal and ventral NSCs in any of the readouts were observed across multiple studies. Following 72 hours of treatment with BMP4, Ki67 was decreased, and VCAM1 increased, in ventral NSCs grown in media containing BMP4/FGF-2 compared to controls (Fig 6A and 6B). These data suggest that exposure to BMP4 had a comparable effect inducing quiescence in both ventral NSCs and dorsal NSCs. Following 72 hours of BMP4 exposure, median levels of p-STAT3 S727 (Fig 6C) and p-4EBP1/2 T37/46 (Fig 6F) both decreased compared to ventral cells grown in EGF/FGF-2 media as they did in dorsal cells exposed to BMP4. However, as in dorsal NSCs, in ventral NSCs, levels of p-S6 S235/236 (Fig 6D) and p-S6 S240/244 (Fig 6E) did not change following 72 hours in culture with BMP4.

Discussion

In both the ventricular-subventricular zone and the dentate gyrus of the hippocampus, temporary quiescence of a subset of embryonic neural stem cells determines the capacity of the adult neurogenic niche through preservation of self-renewing stem cells that later activate in the adult. Lineage tracing work in rodents has shown extensive consequences of altering prenatal quiescence entry in both stem cell niches, including premature depletion of the postnatal stem cell population and developmental and learning defects (D. Y. Wang et al., 2020; Hu et al., 2017; Kokovay et al., 2012). This quiescence entry is thus essential to produce adult neural stem cells and support adult neurogenesis in both the V-SVZ and dentate gyrus. However, the mechanisms regulating the initiation of this essential process remain poorly understood (Urbán, 2022; Urbán et al., 2019).

mTOR has been shown to regulate the balance of activation and quiescence in other stem cell populations (Cho & Hwang, 2012; Nieto-González et al., 2019; Rodgers et al., 2014). In postnatal NSCs, mTOR also regulates preferential translation of specific mRNA transcripts as stem cells are activated to divide – that is, upon exit from quiescence (Baser et al., 2019; Rossi et al., 2021). The data shown here illuminate a role for this kinase in embryonic NSC quiescence. While the sufficiency of changes in p-4EBP1/2 for initiation of quiescence entry is demonstrated here, the necessity and sufficiency of increased p-4EBP1/2 for quiescence exit in these cells remain to be explored. Nutrient sensing and PI3K/Akt signaling upstream of mTOR have been proposed as a regulator of NSC quiescence exit (Chell & Brand, 2010). Whether mTOR-mediated phosphorylation of 4EBP1/2 is a regulator of both quiescence entry and exit or how it may work coordinately with other signaling pathways well known to be involved in quiescence, such as Notch signaling, is an area of ongoing study.

These data demonstrate that two primary downstream effectors of mTORC1, p-S6 S240/244 and p-4EBP1/2 T37/46, have distinct patterns of expression throughout neurogenesis and rarely appear in

the same cell (fewer than 1% of cells at E15 and E17). Cells positive for p-4EBP1/2 line the most apical portion of the developing telencephalon, the ventricular zone, and their abundance decreases with age, while cells positive for p-S6 predominate in the subventricular zone, intermediate zone, and cortical plate and their abundance increases with age. The finding that p-4EBP1/2 and p-S6 were so rarely expressed in the same cell indicates that though the mTOR pathway is active in both cells, through a yet unidentified regulatory mechanism, only one signaling effector is being phosphorylated. While it has been reported that different ligands (such as amino acids, insulin, and growth factors) activating different upstream receptors (including the epidermal growth factor receptor, the fibroblast growth factor receptor, and the insulin receptor) can result in various downstream signaling responses (Sparta et al., 2021), it remains to be explored whether this type of mechanism is responsible for the differing patterns of phosphorylation of these two key mTORC1 effectors in NSCs.

The use of BMP4 in embryonic NSC cultures resulted in decreased expression of Ki67, increased expression of VCAM1, an increased percentage of cells in the G0/G1 phase of the cell cycle and decreased percentages of cells in the S and G2/M phases of the cell cycle. Cells exposed to BMP4 did not enter senescence (data not shown). Upon quiescence entry, levels of p-4EBP1/2, but not p-S6, decreased in cultures derived from the developing dorsal region. The wider variance seen in S6 signaling may reflect its role in additional biological processes, such as regulating cell size (Hartman et al., 2013; Magnuson et al., 2012; Montagne et al., 1999; Ruvinsky & Meyuhas, 2006). In concordance with the effects of BMP4, inhibition of p-4EBP1/2, but not p-S6, was sufficient to induce quiescence entry. Importantly, while levels of another mTOR downstream effector, p-STAT3, decreased in both dorsal and ventral NSCs exposed to BMP4, it did not decrease upon entry into quiescence after 24 hours with RapaLink treatment while cells had already begun to exit the cell cycle and quiesce. The opposing relationships of BMP and STAT3 signaling through mTOR to influence stem cell fate have been previously described (Rajan et al., 2003). The data here indicate the inhibition of phosphorylation of STAT3 is not

559 necessary for quiescence entry and may be a secondary consequence, whereas mTOR-dependent
560 phosphorylation of 4EBP1/2 is a regulator of embryonic NSC quiescence entry.

561 While p-4EBP1/2 positive cells were nearly always dividing and co-expressed Ki67, p-S6 positive
562 cells co-expressed Ki67 only 30% of the time, on average. This pattern may offer insight into the
563 independent biological functions that activation of each signaling protein triggers and the consequences
564 on stem cell proliferation, self-renewal, and differentiation those functions have. It has been widely
565 reported that as stem cells differentiate and migrate tangentially away from the ventricular surface,
566 translation is suppressed. This suppression of translation, and regulation of the process by mTOR, has
567 been hypothesized to be a mechanism of regulating stem cell fate (reviewed in R. Wang & Amoyel,
568 2022). mTOR-mediated translation of specific transcripts – or lack thereof – during key periods of
569 neurogenesis has been shown to regulate cellular differentiation and neuronal subtype specification
570 (Harnett et al., 2022; reviewed in Statoulla et al., 2021). The data presented here support this
571 hypothesis, as p-4EBP1/2, a key regulator of translation, decreases with increasing distance from the
572 ventricular surface and as embryonic development proceeds. These data also offer a new insight into
573 the role of p-S6 in stem cell differentiation to be explored in future studies, as p-S6 is markedly absent at
574 the ventricular surface but its abundance increases with increasing distance from the ventricular
575 surface.

576 An important implication of these data is that each downstream effector of mTOR should be
577 investigated independent of the other signaling molecules in each cell type. mTOR signaling has been
578 implicated as a proposed regulatory mechanism in multiple aspects of neural development and a variety
579 of diseases of the nervous system (Andrews et al., 2020; Avet-Rochex et al., 2014; Costa-Mattioli &
580 Monteggia, 2013; D'Gama et al., 2017; Hartman et al., 2013; Ka et al., 2014; Lee, 2015; Licausi &
581 Hartman, 2018; D. Liu et al., 2018; Mahoney et al., 2016; Maierbrugger et al., 2020; Musah et al., 2020;
582 Paliouras et al., 2012; Rushing et al., 2019; Tee et al., 2016; Tyler et al., 2009; Wahl et al., 2014; Zeng et

583 al., 2009). Often, however, only a single residue on p-S6 – either S235/236 or S240/244 – is reported as
584 a representative readout of total mTOR kinase activity. The data here demonstrate that the multiple
585 signaling effectors of mTORC1 behave independently in tissue, *in vitro*, and in response to different
586 pharmacological modulators. More broadly, as multiple generations of mTOR inhibitors enter clinical
587 trials, the use of agents that more effectively inhibit phosphorylation of both S6 and 4EBP1/2 are likely
588 to have broader effects on normal neural development, and cortical hyperplasias, than their
589 predecessors.

590 Three different generations of mTOR inhibitors were tested here for their ability to inhibit
591 phosphorylation of 4EBP1/2. While the inhibitors tested have all been reported to decrease p-4EBP1/2
592 levels in cell lines and *in vitro* assays, only the third-generation bivalent inhibitor, RapaLink-1, was able
593 to decrease levels of p-4EBP1/2 in embryonic neural stem cell cultures. Rapamycin, a first-generation
594 inhibitor, multiple second-generation "Tork" inhibitors, and a eukaryotic initiation factor inhibitor all
595 failed to decrease levels of p-4EBP1/2. The data presented here may indicate cell type-specific
596 mechanisms regulating mTOR signaling and susceptibility to inhibition. This finding has potential
597 implications for clinical use, where mTOR inhibitors are often prescribed for a variety of diseases. First
598 generation mTOR inhibitors (rapalogs) are often prescribed for pediatric patients with "mTORopathies,"
599 a debilitating class of neurodevelopmental disorders. Patients with tuberous sclerosis complex, one such
600 mTORopathy wherein patients have tumors throughout the entire body, are regularly prescribed the
601 rapalog everolimus to control seizures and limit brain tumor growth (Cavalheiro et al., 2021; Feliciano,
602 2020; Franz, 2011; Karalis & Bateup, 2021; Overwater et al., 2019). This work may indicate that only the
603 S6 "arm" of the mTOR pathway is inhibited by rapalog treatment and may offer insight as to why such
604 treatments are not cytotoxic, but merely cytostatic. These data support the testing of improved mTOR
605 inhibitors that more effectively inhibit phosphorylation of 4EBP1/2 in neural stem cells, but also raise
606 concern that this targeting may incur additional side effects.

An additional area of future study is the comparison to the human brain. The day 10 neurospheres derived from human iPSCs presented here suggest the independent phosphorylations of S6 and 4EBP1/2 also occur in human cells. Outer radial glial cells, a cell type unique to the human brain hypothesized to be a cell of origin in disease, have been reported to have increased mTOR activity, as measured by p-S6, compared to other types of cells (Andrews et al., 2020; Nowakowski et al., 2017). Embryonic neural stem cells have been hypothesized to be the cell of origin for some of the brain tumor types found in tuberous sclerosis complex (Blair et al., 2018; Eichmüller et al., 2022; Hang et al., 2017; Hewer & Vajtai, 2015; Rushing et al., 2019). However, more work is needed to determine whether there are changes in mTOR-dependent phosphorylation of 4EBP1/2 upon quiescence entry in human NSCs. Future studies may investigate how consequences of altered quiescence entry, particularly in the context of disease, may affect a stem cell's lineage and fate.

References

Alvarez-Buylla, A., & García-Verdugo, J. M. (2002). Neurogenesis in adult subventricular zone. In *Journal of Neuroscience* (Vol. 22, Issue 3). https://doi.org/10.1523/jneurosci.22-03-00629.2002

Andrews, M. G., Subramanian, L., & Kriegstein, A. R. (2020). Mtor signaling regulates the morphology and migration of outer radial glia in developing human cortex. *ELife*, *9*. https://doi.org/10.7554/ELIFE.58737

Armstrong, L. C., Westlake, G., Snow, J. P., Cawthon, B., Armour, E., Bowman, A. B., & Ess, K. C. (2017). Heterozygous loss of TSC2 alters p53 signaling and human stem cell reprogramming. *Human Molecular Genetics*, *26*(23). https://doi.org/10.1093/hmg/ddx345

Avet-Rochex, A., Carvajal, N., Christoforou, C. P., Yeung, K., Maierbrugger, K. T., Hobbs, C., Lalli, G., Cagin, U., Plachot, C., McNeill, H., & Bateman, J. M. (2014). Unkempt Is Negatively Regulated by mTOR and Uncouples Neuronal Differentiation from Growth Control. *PLoS Genetics*, *10*(9). https://doi.org/10.1371/journal.pgen.1004624

Baser, A., Skabkin, M., Kleber, S., Dang, Y., Gülcüler Balta, G. S., Kalamakis, G., Göpferich, M., Ibañez, D. C., Schefzik, R., Lopez, A. S., Bobadilla, E. L., Schultz, C., Fischer, B., & Martin-Villalba, A. (2019). Onset of differentiation is post-transcriptionally controlled in adult neural stem cells. *Nature*, *566*(7742). https://doi.org/10.1038/s41586-019-0888-x

Berg, D. A., Su, Y., Jimenez-Cyrus, D., Patel, A., Huang, N., Morizet, D., Lee, S., Shah, R., Ringeling, F. R., Jain, R., Epstein, J. A., Wu, Q. F., Canzar, S., Ming, G. L., Song, H., & Bond, A. M. (2019). A Common Embryonic Origin of Stem Cells Drives Developmental and Adult Neurogenesis. *Cell*, *177*(3). https://doi.org/10.1016/j.cell.2019.02.010

Blair, J. D., Hockemeyer, D., & Bateup, H. S. (2018). Genetically engineered human cortical spheroid models of tuberous sclerosis. *Nature Medicine*, *24*(10). https://doi.org/10.1038/s41591-018-0139-y

Bond, A. M., Ming, G. li, & Song, H. (2021). Ontogeny of adult neural stem cells in the mammalian brain. In *Current Topics in Developmental Biology* (Vol. 142). https://doi.org/10.1016/bs.ctdb.2020.11.002

Cavalheiro, S., da Costa, M. D. S., & Richtmann, R. (2021). Everolimus as a possible prenatal treatment of in utero diagnosed subependymal lesions in tuberous sclerosis complex: a case report. *Child's Nervous System*, *37*(12). https://doi.org/10.1007/s00381-021-05218-4

Chaker, Z., Codega, P., & Doetsch, F. (2016). A mosaic world: puzzles revealed by adult neural stem cell heterogeneity. In *Wiley Interdisciplinary Reviews: Developmental Biology* (Vol. 5, Issue 6). https://doi.org/10.1002/wdev.248

Chalkley, M.-B. L., Mersfelder, R. B., Sundberg, M., Armstrong, L., Sahin, M., Ihrie, R. A., & Ess, K. C. (2022). Non-Canonical Functions of a Mutant TSC2 Protein in Mitotic Division. *BioRxiv*, 2022.12.07.519401. https://doi.org/10.1101/2022.12.07.519401

Chell, J. M., & Brand, A. H. (2010). Nutrition-responsive glia control exit of neural stem cells from quiescence. *Cell*, *143*(7). https://doi.org/10.1016/j.cell.2010.12.007

655 Cho, S., & Hwang, E. S. (2012). Status of mTOR activity may phenotypically differentiate senescence and
656 quiescence. *Molecules and Cells*, *33*(6). https://doi.org/10.1007/s10059-012-0042-1

657 Choi, J., Chen, J., Schreiber, S. L., & Clardy, J. (1996). Structure of the FKBP12-rapamycin complex
658 interacting with the binding domain of human FRAP. *Science*, *273*(5272).
659 https://doi.org/10.1126/science.273.5272.239

660 Costa-Mattioli, M., & Monteggia, L. M. (2013). mTOR complexes in neurodevelopmental and
661 neuropsychiatric disorders. In *Nature Neuroscience* (Vol. 16, Issue 11).
662 https://doi.org/10.1038/nn.3546

663 David-Bercholz, J., Kuo, C. T., & Deneen, B. (2021). Astrocyte and Oligodendrocyte Responses From the
664 Subventricular Zone After Injury. In *Frontiers in Cellular Neuroscience* (Vol. 15).
665 https://doi.org/10.3389/fncel.2021.797553

666 Delgado, A. C., Maldonado-Soto, A. R., Silva-Vargas, V., Mizrak, D., von Känel, T., Tan, K. R., Paul, A.,
667 Madar, A., Cuervo, H., Kitajewski, J., Lin, C. S., & Doetsch, F. (2021). Release of stem cells from
668 quiescence reveals gliogenic domains in the adult mouse brain. *Science*, *372*(6547).
669 https://doi.org/10.1126/science.abg8467

670 D'Gama, A. M., Woodworth, M. B., Hossain, A. A., Bizzotto, S., Hatem, N. E., LaCoursiere, C. M., Najm, I.,
671 Ying, Z., Yang, E., Barkovich, A. J., Kwiatkowski, D. J., Vinters, H. v., Madsen, J. R., Mathern, G. W.,
672 Blümcke, I., Poduri, A., & Walsh, C. A. (2017). Somatic Mutations Activating the mTOR Pathway in
673 Dorsal Telencephalic Progenitors Cause a Continuum of Cortical Dysplasias. *Cell Reports*, *21*(13).
674 https://doi.org/10.1016/j.celrep.2017.11.106

675 Dodd, K. M., Yang, J., Shen, M. H., Sampson, J. R., & Tee, A. R. (2015). mTORC1 drives HIF-1α and VEGF-A
676 signalling via multiple mechanisms involving 4E-BP1, S6K1 and STAT3. *Oncogene*, *34*(17).
677 https://doi.org/10.1038/onc.2014.164

678 Doetsch, F., García-Verdugo, J. M., & Alvarez-Buylla, A. (1997). Cellular composition and three-
679 dimensional organization of the subventricular germinal zone in the adult mammalian brain.
680 *Journal of Neuroscience*, *17*(13). https://doi.org/10.1523/jneurosci.17-13-05046.1997

681 Ebrahimi-Fakhari, D., Stires, G., Hahn, E., Krueger, D., & Franz, D. N. (2021). Prenatal Sirolimus Treatment
682 for Rhabdomyomas in Tuberous Sclerosis. *Pediatric Neurology*, *125*.
683 https://doi.org/10.1016/j.pediatrneurol.2021.09.014

684 Eichmüller, O. L., Corsini, N. S., Vértesy, Á., Morassut, I., Scholl, T., Gruber, V. E., Peer, A. M., Chu, J.,
685 Novatchkova, M., Hainfellner, J. A., Paredes, M. F., Feucht, M., & Knoblich, J. A. (2022).
686 Amplification of human interneuron progenitors promotes brain tumors and neurological defects.
687 *Science*, *375*(6579). https://doi.org/10.1126/science.abf5546

688 Englund, C., Fink, A., Lau, C., Pham, D., Daza, R. A. M., Bulfone, A., Kowalczyk, T., & Hevner, R. F. (2005).
689 Pax6, Tbr2, and Tbr1 are expressed sequentially by radial glia, intermediate progenitor cells, and
690 postmitotic neurons in developing neocortex. *Journal of Neuroscience*, *25*(1).
691 https://doi.org/10.1523/JNEUROSCI.2899-04.2005

692 Fan, Q. W., Aksoy, O., Wong, R. A., Ilkhanizadeh, S., Novotny, C. J., Gustafson, W. C., Truong, A. Y. Q.,
693 Cayanan, G., Simonds, E. F., Haas-Kogan, D., Phillips, J. J., Nicolaides, T., Okaniwa, M., Shokat, K. M.,
694 & Weiss, W. A. (2017). A Kinase Inhibitor Targeted to mTORC1 Drives Regression in Glioblastoma.
695 *Cancer Cell*, *31*(3). https://doi.org/10.1016/j.ccell.2017.01.014

696 Fan, Q. W., Nicolaides, T. P., & Weiss, W. A. (2018). Inhibiting 4EBP1 in glioblastoma. In *Clinical Cancer*
697 *Research* (Vol. 24, Issue 1). https://doi.org/10.1158/1078-0432.CCR-17-0042

698 Feldman, M. E., Apsel, B., Uotila, A., Loewith, R., Knight, Z. A., Ruggero, D., & Shokat, K. M. (2009).
699 Active-site inhibitors of mTOR target rapamycin-resistant outputs of mTORC1 and mTORC2. *PLoS*
700 *Biology*, *7*(2). https://doi.org/10.1371/journal.pbio.1000038

701 Feliciano, D. M. (2020). The Neurodevelopmental Pathogenesis of Tuberous Sclerosis Complex (TSC). In
702 *Frontiers in Neuroanatomy* (Vol. 14). https://doi.org/10.3389/fnana.2020.00039

703 Franz, D. N. (2011). Everolimus: An mTOR inhibitor for the treatment of tuberous sclerosis. In *Expert*
704 *Review of Anticancer Therapy* (Vol. 11, Issue 8). https://doi.org/10.1586/era.11.93

705 Fuentealba, L. C., Rompani, S. B., Parraguez, J. I., Obernier, K., Romero, R., Cepko, C. L., & Alvarez-Buylla,
706 A. (2015). Embryonic Origin of Postnatal Neural Stem Cells. *Cell*, *161*(7), 1644–1655.
707 https://doi.org/10.1016/j.cell.2015.05.041

708 Furutachi, S., Miya, H., Watanabe, T., Kawai, H., Yamasaki, N., Harada, Y., Imayoshi, I., Nelson, M.,
709 Nakayama, K. I., Hirabayashi, Y., & Gotoh, Y. (2015). Slowly dividing neural progenitors are an
710 embryonic origin of adult neural stem cells. *Nature Neuroscience*, *18*(5).
711 https://doi.org/10.1038/nn.3989

712 Gingras, A. C., Raught, B., & Sonenberg, N. (1999). eIF4 initiation factors: Effectors of mRNA recruitment
713 to ribosomes and regulators of translation. In *Annual Review of Biochemistry* (Vol. 68).
714 https://doi.org/10.1146/annurev.biochem.68.1.913

715 Hang, J. F., Hsu, C. Y., Lin, S. C., Wu, C. C., Lee, H. J., & Ho, D. M. T. (2017). Thyroid transcription factor-1
716 distinguishes subependymal giant cell astrocytoma from its mimics and supports its cell origin from
717 the progenitor cells in the medial ganglionic eminence. *Modern Pathology*, *30*(3).
718 https://doi.org/10.1038/modpathol.2016.205

719 Harnett, D., Ambrozkiewicz, M. C., Zinnall, U., Rusanova, A., Borisova, E., Drescher, A. N., Couce-Iglesias,
720 M., Villamil, G., Dannenberg, R., Imami, K., Münster-Wandowski, A., Fauler, B., Mielke, T., Selbach,
721 M., Landthaler, M., Spahn, C. M. T., Tarabykin, V., Ohler, U., & Kraushar, M. L. (2022). A critical
722 period of translational control during brain development at codon resolution. *Nature Structural &*
723 *Molecular Biology*, *29*(12), 1277–1290. https://doi.org/10.1038/s41594-022-00882-9

724 Hartman, N. W., Lin, T. v., Zhang, L., Paquelet, G. E., Feliciano, D. M., & Bordey, A. (2013). MTORC1
725 Targets the Translational Repressor 4E-BP2, but Not S6 Kinase 1/2, to Regulate Neural Stem Cell
726 Self-Renewal InVivo. *Cell Reports*, *5*(2). https://doi.org/10.1016/j.celrep.2013.09.017

727 Hewer, E., & Vajtai, I. (2015). Consistent nuclear expression of thyroid transcription factor 1 in
728 subependymal giant cell astrocytomas suggests lineage-restricted histogenesis. *Clinical*
729 *Neuropathology*, *34*(3). https://doi.org/10.5414/NP300818

730 Hu, X. L., Chen, G., Zhang, S., Zheng, J., Wu, J., Bai, Q. R., Wang, Y., Li, J., Wang, H., Feng, H., Li, J., Sun, X.,
731 Xia, Q., Yang, F., Hang, J., Qi, C., Phoenix, T. N., Temple, S., & Shen, Q. (2017). Persistent Expression
732 of VCAM1 in Radial Glial Cells Is Required for the Embryonic Origin of Postnatal Neural Stem Cells.
733 *Neuron*, *95*(2). https://doi.org/10.1016/j.neuron.2017.06.047

734 Ihrie, R. A., & Álvarez-Buylla, A. (2011). Lake-Front Property: A Unique Germinal Niche by the Lateral
735 Ventricles of the Adult Brain. In *Neuron* (Vol. 70, Issue 4).
736 https://doi.org/10.1016/j.neuron.2011.05.004

737 Irish, J. M., Myklebust, J. H., Alizadeh, A. A., Houot, R., Sharman, J. P., Czerwinski, D. K., Nolan, G. P., &
738 Levy, R. (2010). B-cell signaling networks reveal a negative prognostic human lymphoma cell subset
739 that emerges during tumor progression. *Proceedings of the National Academy of Sciences of the*
740 *United States of America*, *107*(29). https://doi.org/10.1073/pnas.1002057107

741 Ka, M., Condorelli, G., Woodgett, J. R., & Kim, W. Y. (2014). mTOR regulates brain morphogenesis by
742 mediating GSK3 signaling. *Development (Cambridge)*, *141*(21). https://doi.org/10.1242/dev.108282

743 Karalis, V., & Bateup, H. S. (2021). Current Approaches and Future Directions for the Treatment of
744 mTORopathies. In *Developmental Neuroscience* (Vol. 43, Issues 3–4).
745 https://doi.org/10.1159/000515672

746 Katada, S., Takouda, J., Nakagawa, T., Honda, M., Igarashi, K., Imamura, T., Ohkawa, Y., Sato, S.,
747 Kurumizaka, H., & Nakashima, K. (2021). Neural stem/precursor cells dynamically change their
748 epigenetic landscape to differentially respond to BMP signaling for fate switching during brain
749 development. *Genes and Development*, *35*(21–22). https://doi.org/10.1101/GAD.348797.121

750 Knobloch, M., Pilz, G. A., Ghesquière, B., Kovacs, W. J., Wegleiter, T., Moore, D. L., Hruzova, M.,
751 Zamboni, N., Carmeliet, P., & Jessberger, S. (2017). A Fatty Acid Oxidation-Dependent Metabolic
752 Shift Regulates Adult Neural Stem Cell Activity. *Cell Reports*, *20*(9).
753 https://doi.org/10.1016/j.celrep.2017.08.029

754 Kokovay, E., Wang, Y., Kusek, G., Wurster, R., Lederman, P., Lowry, N., Shen, Q., & Temple, S. (2012).
755 VCAM1 is essential to maintain the structure of the SVZ niche and acts as an environmental sensor
756 to regulate SVZ lineage progression. *Cell Stem Cell*, *11*(2).
757 https://doi.org/10.1016/j.stem.2012.06.016

758 Laplante, M., & Sabatini, D. M. (2012). MTOR signaling in growth control and disease. In *Cell* (Vol. 149,
759 Issue 2). https://doi.org/10.1016/j.cell.2012.03.017

760 Lee, D. Y. (2015). Roles of mTOR Signaling in Brain Development. *Experimental Neurobiology*, *24*(3).
761 https://doi.org/10.5607/en.2015.24.3.177

762 Li, W., Cogswell, C. A., & LoTurco, J. J. (1998). Neuronal differentiation of precursors in the neocortical
763 ventricular zone is triggered by BMP. *Journal of Neuroscience*, *18*(21).
764 https://doi.org/10.1523/jneurosci.18-21-08853.1998

765 Licausi, F., & Hartman, N. W. (2018). Role of mTOR complexes in neurogenesis. In *International Journal*
766 *of Molecular Sciences* (Vol. 19, Issue 5). https://doi.org/10.3390/ijms19051544

767 Lillien, L., & Raphael, H. (2000). BMP and FGF regulate the development of EGF-responsive neural
768 progenitor cells. *Development*, *127*(22). https://doi.org/10.1242/dev.127.22.4993

769 Liu, D., Stowie, A., de Zavalia, N., Leise, T., Pathak, S. S., Drewes, L. R., Davidson, A. J., Amir, S.,
770 Sonenberg, N., & Cao, R. (2018). mTOR signaling in VIP neurons regulates circadian clock synchrony
771 and olfaction. *Proceedings of the National Academy of Sciences of the United States of America*,
772 *115*(14). https://doi.org/10.1073/pnas.1721578115

773 Liu, G. Y., & Sabatini, D. M. (2020). mTOR at the nexus of nutrition, growth, ageing and disease. In
774 *Nature Reviews Molecular Cell Biology* (Vol. 21, Issue 4). https://doi.org/10.1038/s41580-019-
775 0199-y

776 Magnuson, B., Ekim, B., & Fingar, D. C. (2012). Regulation and function of ribosomal protein S6 kinase
777 (S6K) within mTOR signalling networks. In *Biochemical Journal* (Vol. 441, Issue 1).
778 https://doi.org/10.1042/BJ20110892

779 Mahoney, C., Feliciano, D. M., Bordey, A., & Hartman, N. W. (2016). Switching on mTORC1 induces
780 neurogenesis but not proliferation in neural stem cells of young mice. *Neuroscience Letters*, *614*.
781 https://doi.org/10.1016/j.neulet.2015.12.042

782 Maierbrugger, K. T., Sousa-Nunes, R., & Bateman, J. M. (2020). The mTOR pathway component Unkempt
783 regulates neural stem cell and neural progenitor cell cycle in the Drosophila central nervous
784 system. *Developmental Biology*, *461*(1). https://doi.org/10.1016/j.ydbio.2020.01.006

785 Merkle, F. T., Tramontin, A. D., García-Verdugo, J. M., & Alvarez-Buylla, A. (2004). Radial glia give rise to
786 adult neural stem cells in the subventricular zone. *Proceedings of the National Academy of Sciences*
787 *of the United States of America*, *101*(50). https://doi.org/10.1073/pnas.0407893101

788 Mira, H., Andreu, Z., Suh, H., Chichung Lie, D., Jessberger, S., Consiglio, A., Emeterio, J. S., Hortigüela, R.,
789 Marqués-Torrejón, M. Á., Nakashima, K., Colak, D., Götz, M., Fariñas, I., & Gage, F. H. (2010).
790 Signaling through BMPR-IA regulates quiescence and long-term activity of neural stem cells in the
791 adult hippocampus. *Cell Stem Cell*, *7*(1). https://doi.org/10.1016/j.stem.2010.04.016

792 Moghadam, F. H., Sadeghi-Zadeh, M., Alizadeh-Shoorjestan, B., Dehghani-Varnamkhasti, R., Narimani,
793 S., Darabi, L., Esfahani, A. K., & Esfahani, M. H. N. (2018). Isolation and culture of embryonic mouse
794 neural stem cells. *Journal of Visualized Experiments*, *2018*(141). https://doi.org/10.3791/58874

795 Montagne, J., Stewart, M. J., Stocker, H., Hafen, E., Kozma, S. C., & Thomas, G. (1999). Drosophila S6
796 kinase: A regulator of cell size. *Science*, *285*(5436). https://doi.org/10.1126/science.285.5436.2126

797 Musah, A. S., Brown, T. L., Jeffries, M. A., Shang, Q., Hashimoto, H., Evangelou, A. v., Kowalski, A., Batish,
798 M., Macklin, W. B., & Wood, T. L. (2020). Mechanistic target of rapamycin regulates the
799 oligodendrocyte cytoskeleton during myelination. *Journal of Neuroscience*, *40*(15).
800 https://doi.org/10.1523/JNEUROSCI.1434-18.2020

801 Nieto-González, J. L., Gómez-Sánchez, L., Mavillard, F., Linares-Clemente, P., Rivero, M. C., Valenzuela-
802 Villatoro, M., Muñoz-Bravo, J. L., Pardal, R., & Fernández-Chacón, R. (2019). Loss of postnatal
803 quiescence of neural stem cells through mTOR activation upon genetic removal of cysteine string

804 protein-α. *Proceedings of the National Academy of Sciences of the United States of America*,
805 *116*(16). https://doi.org/10.1073/pnas.1817183116

806 Nowakowski, T. J., Bhaduri, A., Pollen, A. A., Alvarado, B., Mostajo-Radji, M. A., di Lullo, E., Haeussler, M.,
807 Sandoval-Espinosa, C., Liu, S. J., Velmeshev, D., Ounadjela, J. R., Shuga, J., Wang, X., Lim, D. A.,
808 West, J. A., Leyrat, A. A., Kent, W. J., & Kriegstein, A. R. (2017). Spatiotemporal gene expression
809 trajectories reveal developmental hierarchies of the human cortex. *Science*, *358*(6368).
810 https://doi.org/10.1126/science.aap8809

811 Obernier, K., & Alvarez-Buylla, A. (2019). Neural stem cells: Origin, heterogeneity and regulation in the
812 adult mammalian brain. In *Development (Cambridge)* (Vol. 146, Issue 4).
813 https://doi.org/10.1242/dev.156059

814 Overwater, I. E., Rietman, A. B., van Eeghen, A. M., & de Wit, M. C. Y. (2019). Everolimus for the
815 treatment of refractory seizures associated with tuberous sclerosis complex (TSC): Current
816 perspectives. In *Therapeutics and Clinical Risk Management* (Vol. 15).
817 https://doi.org/10.2147/TCRM.S145630

818 Paliouras, G. N., Hamilton, L. K., Aumont, A., Joppé, S. E., Barnaб́-Heider, F., & Fernandes, K. J. L. (2012).
819 Mammalian target of rapamycin signaling is a key regulator of the transit-amplifying progenitor
820 pool in the adult and aging forebrain. *Journal of Neuroscience*, *32*(43).
821 https://doi.org/10.1523/JNEUROSCI.2248-12.2012

822 Radecki, D. Z., & Samanta, J. (2022). Endogenous Neural Stem Cell Mediated Oligodendrogenesis in the
823 Adult Mammalian Brain. In *Cells* (Vol. 11, Issue 13). MDPI. https://doi.org/10.3390/cells11132101

824 Rajan, P., Panchision, D. M., Newell, L. F., & McKay, R. D. G. (2003). BMPs signal alternately through a
825 SMAD or FRAP-STAT pathway to regulate fate choice in CNS stem cells. *Journal of Cell Biology*,
826 *161*(5). https://doi.org/10.1083/jcb.200211021

827 Renier, N., Wu, Z., Simon, D. J., Yang, J., Ariel, P., & Tessier-Lavigne, M. (2014). IDISCO: A simple, rapid
828 method to immunolabel large tissue samples for volume imaging. *Cell*, *159*(4).
829 https://doi.org/10.1016/j.cell.2014.10.010

830 Rodgers, J. T., King, K. Y., Brett, J. O., Cromie, M. J., Charville, G. W., Maguire, K. K., Brunson, C., Mastey,
831 N., Liu, L., Tsai, C. R., Goodell, M. A., & Rando, T. A. (2014). MTORC1 controls the adaptive
832 transition of quiescent stem cells from G 0 to GAlert. *Nature*, *510*(7505).
833 https://doi.org/10.1038/nature13255

834 Rodrik-Outmezguine, V. S., Okaniwa, M., Yao, Z., Novotny, C. J., McWhirter, C., Banaji, A., Won, H.,
835 Wong, W., Berger, M., de Stanchina, E., Barratt, D. G., Cosulich, S., Klinowska, T., Rosen, N., &
836 Shokat, K. M. (2016). Overcoming mTOR resistance mutations with a new-generation mTOR
837 inhibitor. *Nature*, *534*(7606). https://doi.org/10.1038/nature17963

838 Rossi, A., Coum, A., Madelenat, M., Harris, L., Miedzik, A., Strohbuecker, S., Chai, A., Fiaz, H., Chaouni, R.,
839 Faull, P., Grey, W., Bonnet, D., Hamid, F., Makeyev, E. v, Snijders, A. P., Kelly, G., Guillemot, F., &
840 Sousa-Nunes, R. (2021). Neural stem cells alter nucleocytoplasmic partitioning and accumulate
841 nuclear polyadenylated transcripts during quiescence. *BioRxiv*, 2021.01.06.425462.
842 https://doi.org/10.1101/2021.01.06.425462

Roux, P. P., Shahbazian, D., Vu, H., Holz, M. K., Cohen, M. S., Taunton, J., Sonenberg, N., & Blenis, J. (2007). RAS/ERK signaling promotes site-specific ribosomal protein S6 phosphorylation via RSK and stimulates cap-dependent translation. *Journal of Biological Chemistry*, *282*(19). https://doi.org/10.1074/jbc.M700906200

Rushing, G. v., Brockman, A. A., Bollig, M. K., Leelatian, N., Mobley, B. C., Irish, J. M., Ess, K. C., Fu, C., & Ihrie, R. A. (2019). Location-dependent maintenance of intrinsic susceptibility to mTORC1-driven tumorigenesis. *Life Science Alliance*, *2*(2). https://doi.org/10.26508/lsa.201800218

Ruvinsky, I., & Meyuhas, O. (2006). Ribosomal protein S6 phosphorylation: from protein synthesis to cell size. In *Trends in Biochemical Sciences* (Vol. 31, Issue 6). https://doi.org/10.1016/j.tibs.2006.04.003

Snow, J. P., Westlake, G., Klofas, L. K., Jeon, S., Armstrong, L. C., Swoboda, K. J., George, A. L., & Ess, K. C. (2020). Neuronal modeling of alternating hemiplegia of childhood reveals transcriptional compensation and replicates a trigger-induced phenotype. *Neurobiology of Disease*, *141*. https://doi.org/10.1016/j.nbd.2020.104881

Sousa-Nunes, R., Yee, L. L., & Gould, A. P. (2011). Fat cells reactivate quiescent neuroblasts via TOR and glial insulin relays in Drosophila. *Nature*, *471*(7339). https://doi.org/10.1038/nature09867

Sparta, B., Pargett, M., Kosaisawe, N., & Albeck, J. G. (2021). Continuous sensing of nutrients and growth factors by the mTORC1-TFEB axis. *BioRxiv*, 2021.08.07.455512. https://doi.org/10.1101/2021.08.07.455512

Spidlen, J., Breuer, K., Rosenberg, C., Kotecha, N., & Brinkman, R. R. (2012). FlowRepository: A resource of annotated flow cytometry datasets associated with peer-reviewed publications. *Cytometry Part A*, *81 A*(9). https://doi.org/10.1002/cyto.a.22106

Statoulla, E., Chalkiadaki, K., Karozis, D., & Gkogkas, C. G. (2021). Regulation of mRNA translation in stem cells; links to brain disorders. In *Cellular Signalling* (Vol. 88). https://doi.org/10.1016/j.cellsig.2021.110166

Sun, Y., Hu, J., Zhou, L., Pollard, S. M., & Smith, A. (2011). Interplay between FGF2 and BMP controls the self-renewal, dormancy and differentiation of rat neural stem cells. *Journal of Cell Science*, *124*(11). https://doi.org/10.1242/jcs.085506

Sundberg, M., Tochitsky, I., Buchholz, D. E., Winden, K., Kujala, V., Kapur, K., Cataltepe, D., Turner, D., Han, M. J., Woolf, C. J., Hatten, M. E., & Sahin, M. (2018). Purkinje cells derived from TSC patients display hypoexcitability and synaptic deficits associated with reduced FMRP levels and reversed by rapamycin. *Molecular Psychiatry*, *23*(11). https://doi.org/10.1038/s41380-018-0018-4

Tee, A. R., Sampson, J. R., Pal, D. K., & Bateman, J. M. (2016). The role of mTOR signalling in neurogenesis, insights from tuberous sclerosis complex. In *Seminars in Cell and Developmental Biology* (Vol. 52). https://doi.org/10.1016/j.semcdb.2016.01.040

Tyler, W. A., Gangoli, N., Gokina, P., Kim, H. A., Covey, M., Levison, S. W., & Wood, T. L. (2009). Activation of the mammalian target of rapamycin (mTOR) is essential for oligodendrocyte differentiation. *Journal of Neuroscience*, *29*(19). https://doi.org/10.1523/JNEUROSCI.0234-09.2009

Urbán, N. (2022). Could a Different View of Quiescence Help Us Understand How Neurogenesis Is Regulated? *Frontiers in Neuroscience*, *16*. https://doi.org/10.3389/fnins.2022.878875

Urbán, N., Blomfield, I. M., & Guillemot, F. (2019). Quiescence of Adult Mammalian Neural Stem Cells: A Highly Regulated Rest. In *Neuron* (Vol. 104, Issue 5). https://doi.org/10.1016/j.neuron.2019.09.026

Wahl, S. E., McLane, L. E., Bercury, K. K., Macklin, W. B., & Wood, T. L. (2014). Mammalian target of rapamycin promotes oligodendrocyte differentiation, initiation and extent of CNS myelination. *Journal of Neuroscience*, *34*(13). https://doi.org/10.1523/JNEUROSCI.4311-13.2014

Wang, D. Y., Luo, A. F., Bai, Q. R., Gong, X. L., Zheng, Y., Shen, Q., Hu, X. L., & Wang, X. M. (2020). VCAM1 Labels a Subpopulation of Neural Stem Cells in the Adult Hippocampus and Contributes to Spatial Memory. *Stem Cell Reports*, *14*(6). https://doi.org/10.1016/j.stemcr.2020.05.012

Wang, R., & Amoyel, M. (2022). mRNA Translation Is Dynamically Regulated to Instruct Stem Cell Fate. *Frontiers in Molecular Biosciences*, *9*. https://doi.org/10.3389/fmolb.2022.863885

Yokogami, K., Wakisaka, S., Avruch, J., & Reeves, S. A. (2000). Serine phosphorylation and maximal activation of STAT3 during CNTF signaling is mediated by the rapamycin target mTOR. *Current Biology*, *10*(1). https://doi.org/10.1016/S0960-9822(99)00268-7

Young, K. M., Fogarty, M., Kessaris, N., & Richardson, W. D. (2007). Subventricular zone stem cells are heterogeneous with respect to their embryonic origins and neurogenic fates in the adult olfactory bulb. *Journal of Neuroscience*, *27*(31). https://doi.org/10.1523/JNEUROSCI.0476-07.2007

Zeng, L. H., Rensing, N. R., & Wong, M. (2009). The mammalian target of rapamycin signaling pathway mediates epileptogenesis in a model of temporal lobe epilepsy. *Journal of Neuroscience*, *29*(21). https://doi.org/10.1523/JNEUROSCI.0066-09.2009

Zhang, Z., Fan, Q., Luo, X., Lou, K., Weiss, W. A., & Shokat, K. M. (2022). Brain-restricted mTOR inhibition with binary pharmacology. *Nature*, *609*(7928). https://doi.org/10.1038/s41586-022-05213-y

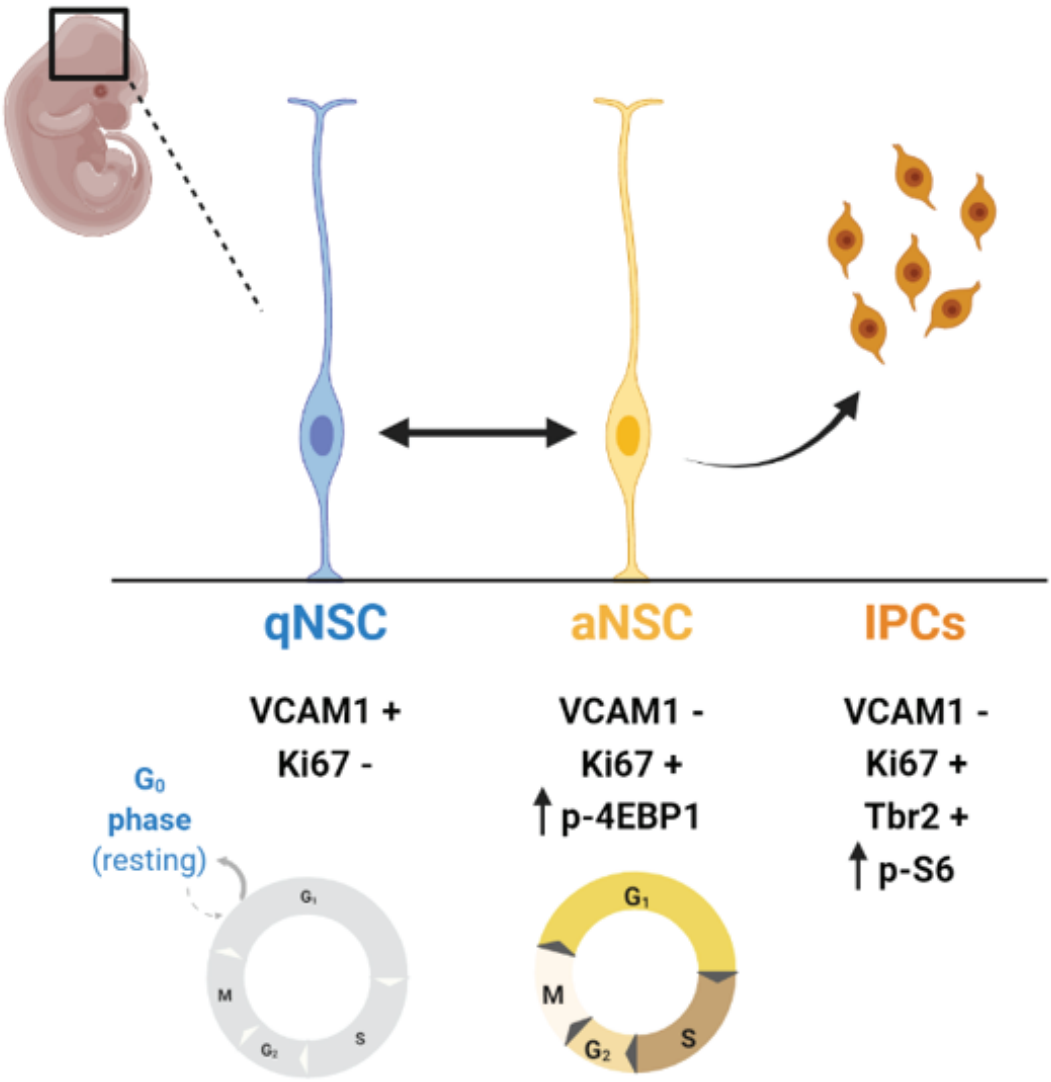

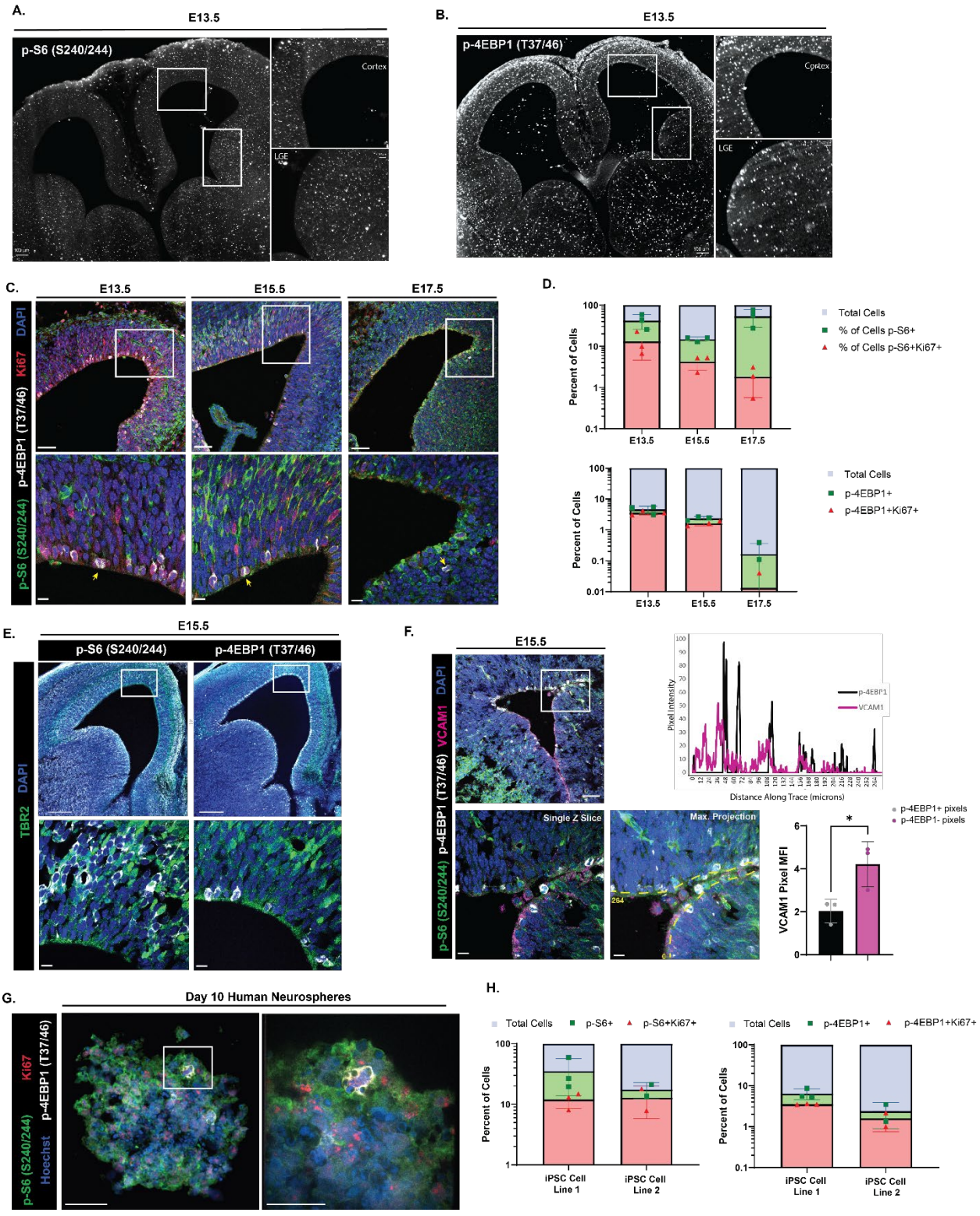

Figure 1: High levels of p-4EBP1/2, but not p-S6, are present in embryonic NSCs at the ventricle. (A) iDISCO+-tissue cleared whole brain from an E13.5 mouse embryo (15X) showing phosphorylation of S6 at

the serine 240/244 residues diffuse throughout the ventricular-subventricular zone tissue in both the developing cortex (inset, top) and lateral ganglionic eminence (inset, bottom). Scale bar information is listed on each figure. (B) iDISCO+-tissue cleared whole brain from an E13.5 mouse embryo (15X) showing phosphorylation of 4EBP1 at the threonine 37/46 residues limited to the cells immediately lining the ventricular surface and not present deeper into the subventricular zone in both the developing cortex (inset, top) and lateral ganglionic eminence (inset, bottom). Scale bar information is listed on each figure. (C) Staining of embryonic mouse brain for the downstream effectors of mTOR at E13.5, E15.5, and E17.5. 20X (top) representative images of the developing ventricular-subventricular zone with single slice of 63X z-stack (bottom) of the inset region showing p-S6 S240/244 (green), p-4EBP1 T37/46 (white), Ki67 (red), and DAPI (blue). Yellow arrows in the 63X representative images mark dividing cells with phosphorylated 4EBP1. Scale bars for all 20X images = 50 µm. Scale bars for all 63X images = 10 µm. (N for E13.5 = 3, N for E15.5 = 4, N for E17.5 = 3) (D) Quantification of the percent of shown in (C) across developmental time points. The percent of all cells positive for p-S6 S240/244 (green) and cells co-positive for p-S6 and Ki67 (red) (top). (2 way ANOVA with Tukey's multiple comparisons test: percent of p-S6 positive cells: E13.5 versus E15.5 $p = 0.0501$, E15.5 versus E17.5 $p = 0.0071$, E13.5 versus E17.5 $p = 0.5377$; percent of p-S6 and Ki67 positive cells: E13.5 versus E15.5 $p = 0.6704$, E15.5 versus E17.5 $p = 0.9697$, E13.5 versus E17.5 $p = 0.5301$). The percent of all cells positive for p-4EBP1 T37/46 (green) and cells co-positive for p-4EBP1 and Ki67 (red) (bottom). (2 way ANOVA with Tukey's multiple comparisons test: percent of p-4EBP1 positive cells: E13.5 versus E15.5 $p = 0.0022$, E15.5 versus E17.5 $p = 0.0023$, E13.5 versus E17.5 $p < 0.0001$; percent of p-4EBP1 and Ki67 positive cells: E13.5 versus E15.5 $p = 0.0056$, E15.5 versus E17.5 $p = 0.0184$, E13.5 versus E17.5 $p < 0.0001$). Error bars represent standard deviation. Plots showing statistics with significance shown in Extended Figure 1-1. (E) Staining of E15.5 mouse brain for the downstream effectors of mTOR and marker of intermediate progenitor cells. 5X representative images (top) of the developing ventricular-subventricular zone with single slice of 63X z-stack (bottom) of the inset region showing Tbr2

(green) colocalizing with p-S6 S240/244 (white, left) but not with p-4EBP1 T37/46 (white, right), and DAPI (blue). Scale bars for 5X images = 200 µm. Scale bars for 63X images = 10 µm. (F) Staining of E15.5 mouse brain for the downstream effectors of mTOR and protein required for radial glia maintenance and quiescence entry. 20X representative image (top left) of the developing ventricular-subventricular zone with single slice of 63X z-stack (bottom left) of the inset region showing p-S6 S240/244 (green), p-4EBP1 T37/46 (white), VCAM1 (magenta), and DAPI (blue). Line trace reporting pixel intensity for p-4EBP1 T37/46 (black) and VCAM1 (magenta) across distance of yellow dashed line shown in maximum projection image of the z stack for the inset region (top right). Maximum projection image of the z stack for the inset region (bottom middle). Quantification of the median fluorescence intensity of VCAM1 in pixels positive for p-4EBP1 (black) versus pixels negative for p-4EBP1 (magenta) (bottom right). Error bars represent standard deviation. (N = 3, paired two-tailed t test p value = 0.0175). Scale bars for 20X image = 50 µm. Scale bars for 63X images = 10 µm. (G) Staining of a wild type day 10 neurosphere derived from human induced pluripotent stem cells for the downstream effectors of mTOR. 40X (left) representative image of sphere within organoid with 100X image of the inset region (right) showing a dividing cell expressing p-S6 S240/244 (green), p-4EBP1 T37/46 (white), Ki67 (red), and Hoechst (blue). Scale bars for both images = 50 µm. (N = 2 representing 2 unique differentiations of 2 independent sets of wild type iPSC lines.) (H) Quantification of the percent of shown in (G) of day 10 cortical organoids. The percent of all cells positive for p-S6 S240/244 (green) and cells co-positive for p-S6 and Ki67 (red) (left). The percent of all cells positive for p-4EBP1 T37/46 (green) and cells co-positive for p-4EBP1 and Ki67 (red) (right). Error bars represent standard deviation.

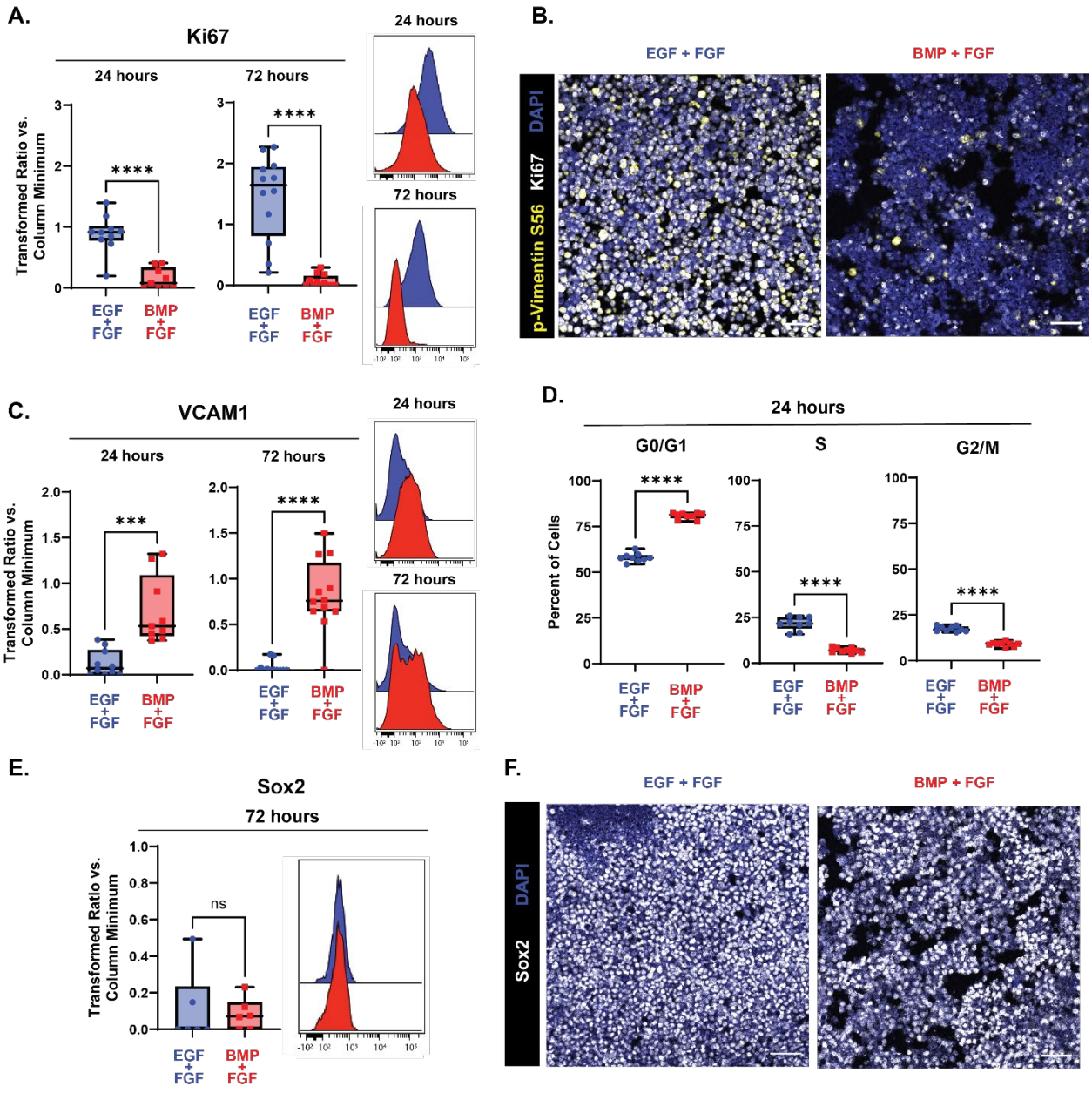

Figure 2: Exposure to BMP4 induces quiescence in embryonic NSCs *in vitro*. Quantification of proliferation and quiescence markers in E15.5 NSC cultures grown for 24 (left in plots) and 72 (right in plots) hours with media containing EGF/FGF (blue) or BMP4/FGF (red). For all plots, the Y axis depicts the arcsinh transformed ratio versus column minimum for a particular antigen. A difference of 0.4 corresponds to an approximately 2-fold difference of total protein. Representative histograms of 24 (top) and 72 hours (bottom). For all plots, error bars contact the maximum and minimum values. For Ki67 and

VCAM1, at 24 hours N = 10 for EGF/FGF, N = 9 for BMP4/FGF; at 72 hours N = 12. (A) Quantification of levels of Ki67 (24 hours: unpaired two-tailed t- test $p < 0.0001$; 72 hours: unpaired two-tailed t-test $p < 0.0001$). (B) 20X representative images of E15.5 NSCs cultured in media with EGF/FGF (left) or BMP4/FGF (right) for p-vimentin S56 (yellow), Ki67 (white), and DAPI (blue). (C) Quantification of levels of VCAM1 (24 hours: unpaired two-tailed t- test $p = 0.0003$; 72 hours: unpaired two-tailed t-test $p < 0.0001$). (D) Percent of E15.5 NSC cultures grown for 24 hours with media containing EGF/FGF (blue) or BMP4/FGF (red) in each phase of the cell cycle. (N = 9, G0/G1 phase unpaired two-tailed t-test $p < 0.0001$, S phase unpaired two-tailed t-test $p < 0.0001$, G2/M unpaired two-tailed t-test $p < 0.0001$). (E) Quantification of levels of Sox2 (N = 6, Mann-Whitney test $p = 0.6688$). (F) 20X representative images of E15.5 NSCs cultured in media with EGF/FGF (left) or BMP4/FGF (right) stained for Sox2 (white) and DAPI (blue). Scale bars for all 20X images = 50 µm.

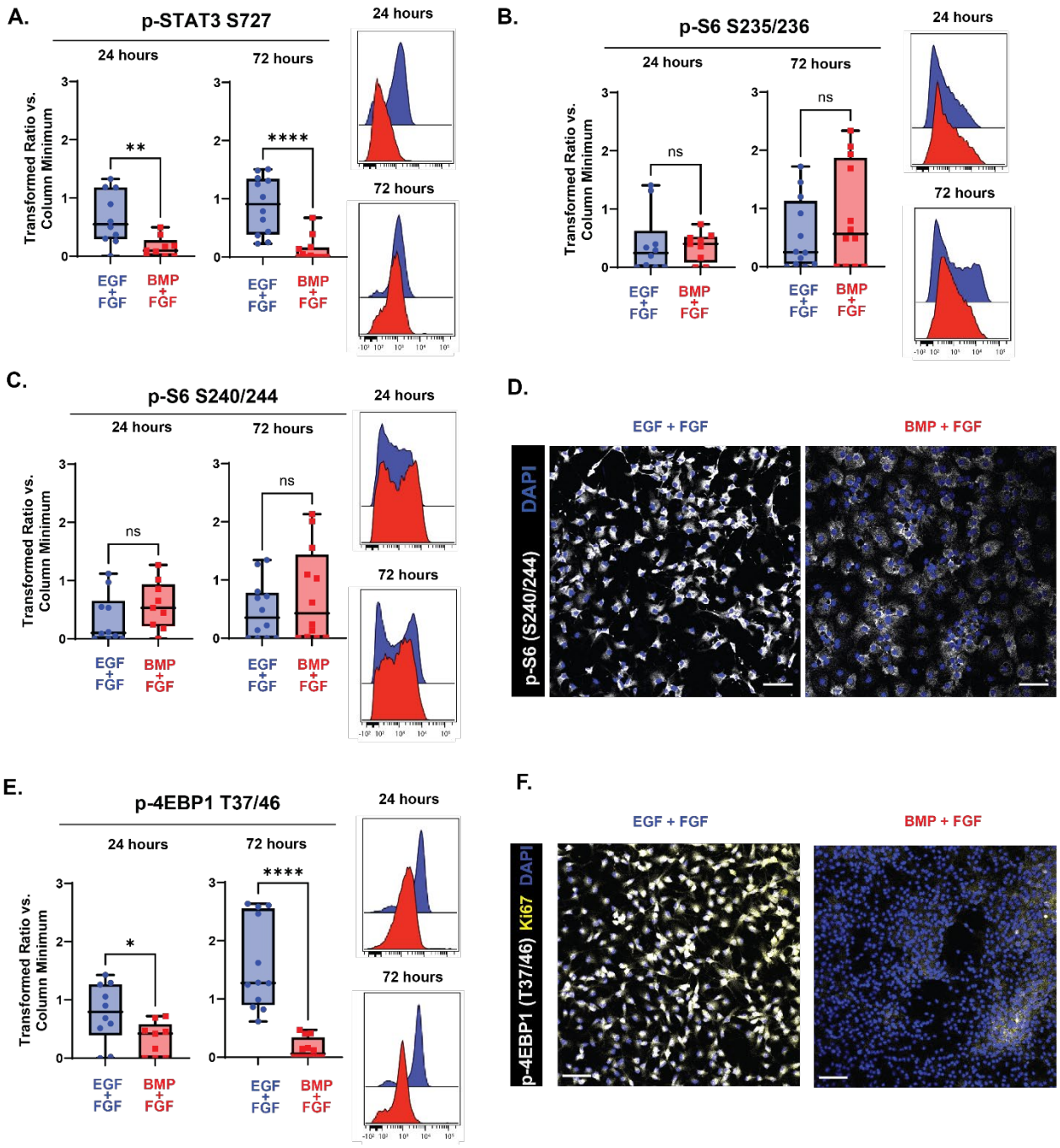

Figure 3: p-4EBP1/2 signaling decreases in embryonic NSCs following quiescence induction. Quantification of effectors downstream of mTOR in E15.5 NSC cultures grown for 24 (left in plots) and 72 (right in plots) hours with media containing EGF/FGF (blue) or BMP4/FGF (red). For all plots, the Y axis depicts the arcsinh transformed ratio versus column minimum for a particular antigen. A difference of 0.4 corresponds to an approximately 2-fold difference of total protein. Representative histograms of 24 (top)

and 72 hours (bottom). For all plots, error bars contact the maximum and minimum values. For all antigens, at 24 hours N = 10 for EGF/FGF, N = 9 for BMP4/FGF; at 72 hours N = 12. (A) Quantification of levels of p-STAT3 S727 (24 hours: unpaired two-tailed t-test $p = 0.0063$; 72 hours: Mann-Whitney test $p < 0.0001$). (B) Quantification of levels of p-S6 S235/236 (24 hours: unpaired two-tailed t-test $p = 0.8102$; 72 hours: unpaired two-tailed t-test $p = 0.3159$). (C) Quantification of levels of p-S6 S240/244 (24 hours: unpaired two-tailed t-test $p = 0.2393$; 72 hours: unpaired two-tailed t-test $p = 0.3461$). (D) 20X representative images of E15.5 NSCs cultured for 6 days in media with EGF/FGF (left) or BMP4/FGF (right) stained for p-S6 S240/244 (white) and DAPI (blue). (E) Quantification of levels of p-4EBP1 T37/46 (24 hours: unpaired two-tailed t-test $p = 0.0318$; 72 hours: unpaired two-tailed t-test $p < 0.0001$). (F) 20X representative images of E15.5 NSCs cultured for 6 days in media with EGF/FGF (left) or BMP4/FGF (right) stained for p-4EBP1 T37/46 (white), Ki67 (yellow) and DAPI (blue). Scale bars for all 20X images = 50 µm.

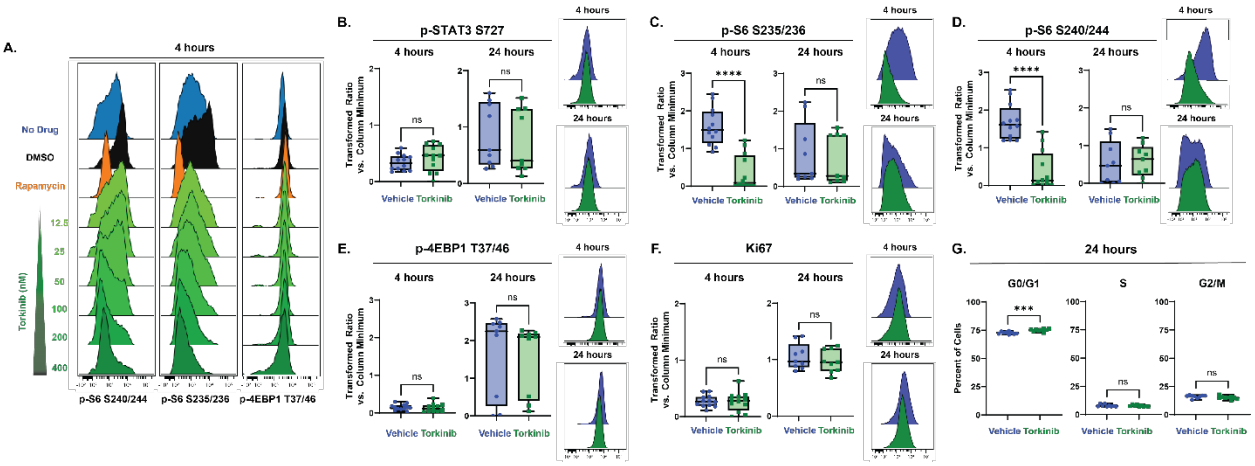

93

94 **Figure 4: Decreases in mTOR-dependent phosphorylation of S6 are not sufficient to induce quiescence.**

95 (A) Representative histograms downstream effectors of mTOR from a dose-response experiment
96 comparing E15.5 NSCs untreated (blue) to E15.5 NSCs treated with DMSO (0.06%, black), Rapamycin (30
97 nM, orange), or Torkinib (12.5 – 400 nM, green). Quantification of proliferation markers and effectors
98 downstream of mTOR in E15.5 NSC cultures treated for 4 (left in plots) and 24 (right in plots) hours with
99 media vehicle (1X PBS, blue) or 400 nM Torkinib (green). For all plots, the Y axis depicts the arcsinh
100 transformed ratio versus column minimum for a particular antigen. A difference of 0.4 corresponds to an
101 approximately 2-fold difference of total protein. Representative histograms of 4 (top) and 24 hours
102 (bottom). For all plots, error bars contact the maximum and minimum values. For all antigens, at 4 hours,
103 N = 12; at 24 hours, N =9. (B) Quantification of levels of p-STAT3 S727 (4 hours: unpaired two-tailed t-test
104 p = 0.3123; 24 hours: unpaired two-tailed t-test p = 0.6878). (C) Quantification of levels of p-S6 S235/236
105 (4 hours: unpaired two-tailed t-test $p < 0.0001$; 24 hours: Mann-Whitney test p = 0.5457). (D)
106 Quantification of levels of p-S6 S240/244 (4 hours: unpaired two-tailed t-test $p < 0.0001$; 24 hours:
107 unpaired two-tailed t-test p = 0.8272). (E) Quantification of levels of p-4EBP1 T37/46 (4 hours: unpaired
108 two-tailed t-test p = 0.5915; 24 hours: unpaired two-tailed t-test p = 0.8275). (F) Quantification of levels
109 of Ki67 (4 hours: unpaired two-tailed t-test p = 0.8409; 24 hours: unpaired two-tailed t-test p = 0.4361).
110 (G) Percent of E15.5 NSC cultures treated for 24 hours 400 nM Torkinib in each phase of the cell cycle. (N

111 = 9; G0/G1 phase unpaired two-tailed t-test p = 0.0005, S phase unpaired two-tailed t-test p = 0.7134,

112 G2/M unpaired two-tailed t-test p = 0.1695).

113

114

115

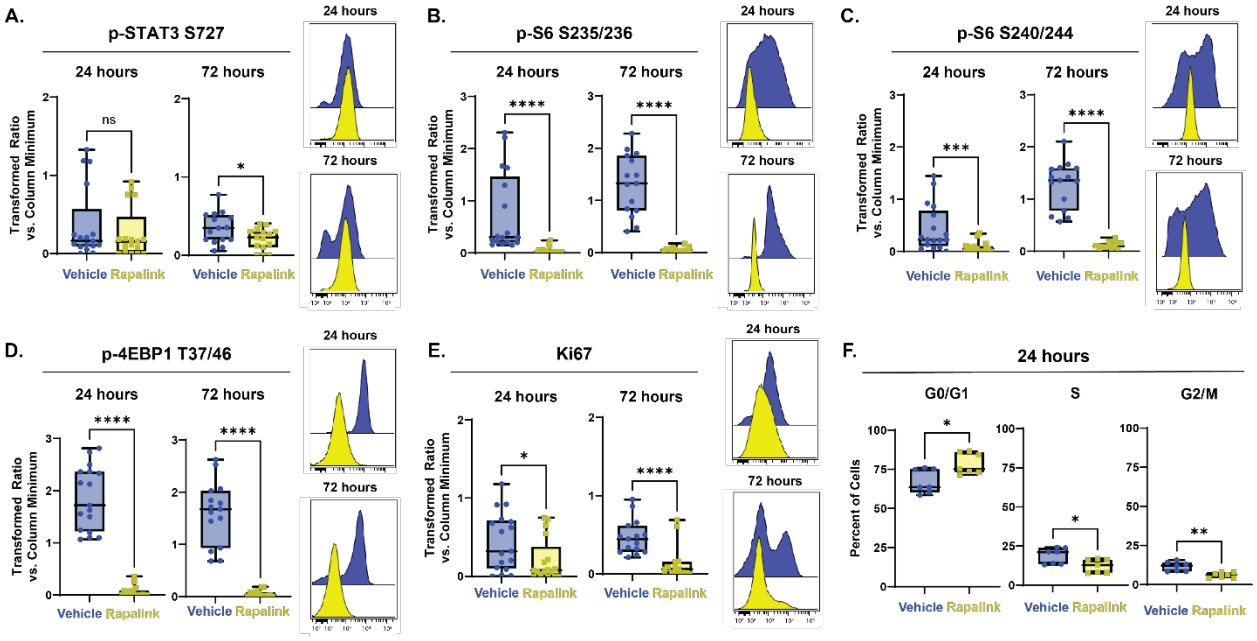

Figure 5: Decreases in mTOR-dependent phosphorylation of 4EBP1/2 are sufficient to induce quiescence. Quantification of proliferation markers and effectors downstream of mTOR in E15.5 NSC cultures treated for 24 (left in plots) and 72 (right in plots) hours with media vehicle (1X PBS, blue) or 10 nM RapaLink (yellow). For all plots, the Y axis depicts the arcsinh transformed ratio versus column minimum for a particular antigen. A difference of 0.4 corresponds to an approximately 2-fold difference of total protein. Representative histograms of 24 (top) and 72 hours (bottom). For all plots, error bars contact the maximum and minimum values. For all antigens, at 24 hours N = 17; at 72 hours N = 15. (A) Quantification of levels of p-STAT3 S727 (24 hours: unpaired two-tailed t-test p = 0.4550; 72 hours: unpaired two-tailed t-test p = 0.0330). (B) Quantification of levels of p-S6 S235/236 (24 hours: Mann-Whitney test p < 0.0001; 72 hours unpaired two-tailed t-test p < 0.0001). (C) Quantification of levels of p-S6 S240/244 (24 hours: Mann-Whitney test p = 0.0009; 72 hours: unpaired two-tailed t-test p < 0.0001). (D) Quantification of levels of p-4EBP1 T37/46 (24 hours: Mann-Whitney test p < 0.0001; 72 hours: unpaired two-tailed t-test p < 0.0001). (E) Quantification of levels of Ki67 (24 hours: unpaired two-tailed t-test p = 0.0433; 72 hours: Mann-Whitney test p < 0.0001). (F) Percent of E15.5 NSC cultures treated for

24 hours 10 nM RapaLink in each phase of the cell cycle. (N = 7, G0/G1 phase unpaired two-tailed t-test p = 0.0126, S phase unpaired two-tailed t-test p = 0.0223, G2/M unpaired two-tailed t-test p = 0.0011).

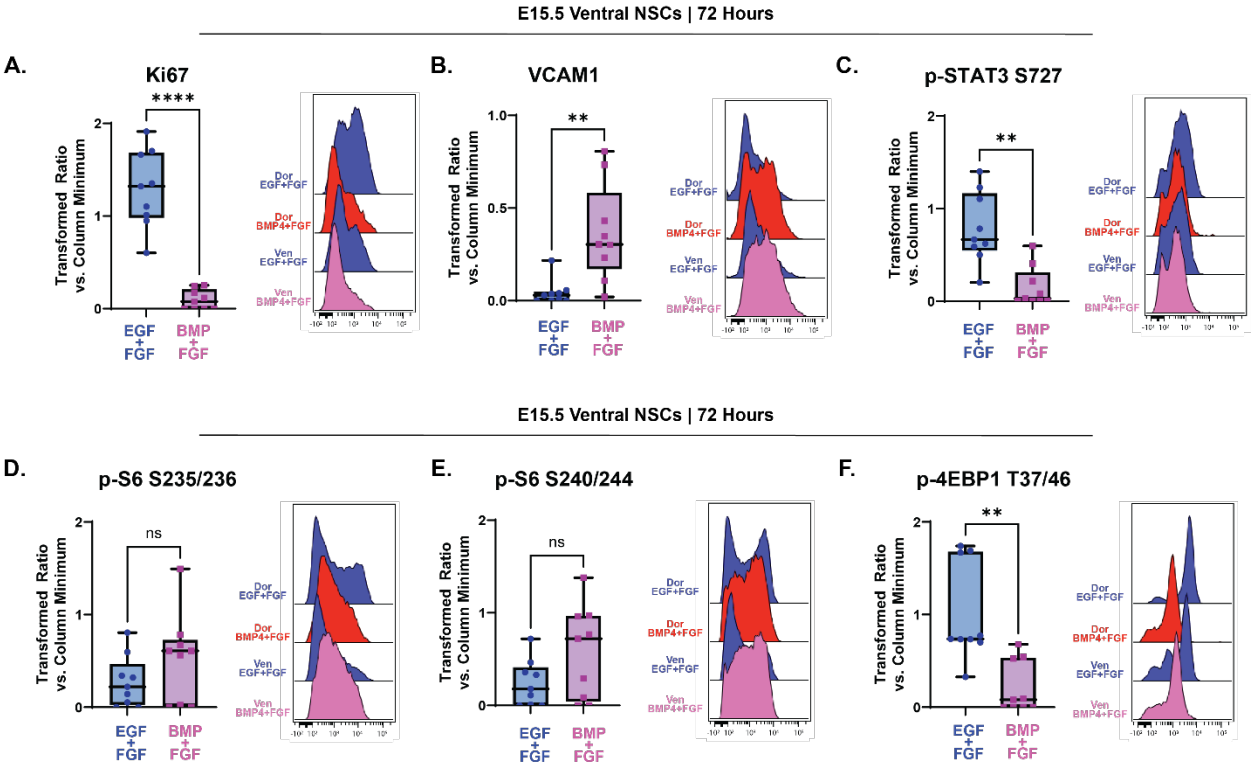

Figure 6: Quiescence entry and mTOR response do not differ by dorsoventral position. Quantification of effectors downstream of mTOR in E15.5 NSC ventral cultures grown 72 hours with media containing EGF/FGF (blue) or BMP4/FGF (pink). For all plots, the Y axis depicts the arcsinh transformed ratio versus column minimum for a particular antigen. A difference of 0.4 corresponds to an approximately 2-fold difference of total protein. Representative histograms comparing E15.5 dorsal and ventral NSC cultures grown in EGF/FGF media or BMP4/FGF media for 72 hours. For all plots, error bars contact the maximum and minimum values. For all antigens, N = 9. (A) Quantification of levels of Ki67 (paired two-tailed t-test $p < 0.0001$). (B) Quantification of levels of VCAM1 (Wilcoxon matched-pairs signed rank test $p = 0.0039$). (C) Quantification of levels of p-STAT3 S727 (paired two-tailed t-test $p = 0.0015$). (D) Quantification of levels of p-S6 S235/236 (paired two-tailed t-test $p = 0.1707$). (E) Quantification of levels of p-S6 S240/244 (paired two-tailed t-test $p = 0.1871$). (F) Quantification of levels of p-4EBP1 T37/46 (paired two-tailed t-test $p = 0.0053$).